**Abstract** Quadratic nonlinear photonic crystals are materials in which the second order susceptibility $\chi^{(2)}$ is spatially modulated while the linear susceptibility remains constant. These structures are significantly different than the more common photonic crystals, in which the linear susceptibility is modulated. Nonlinear processes in nonlinear photonic crystals are governed by the phase matching requirements, which are determined by the reciprocal lattice of these crystals. Therefore, the modulation of the nonlinear susceptibility enables to engineer the spatial and spectral response in various three-wave mixing processes. It enables to support the efficient generation of new optical frequencies at multiple directions. We analyze three wave mixing processes in nonlinear photonic crystals in which the modulation is either periodic, quasi-periodic, radially symmetric or even random. We discuss both one-dimensional and two-dimensional modulations. In addition to harmonic generations, we outline several new possibilities for all-optical control of the spatial and polarization properties of optical beams in specially designed nonlinear photonic crystals.
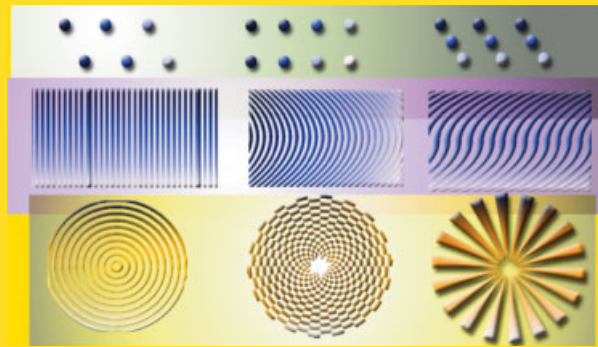
Some examples of nonlinear photonic crystals. Top line: 2D Periodic crystals; center line: 1D quasi-periodic crystals, symmetric and anti-symmetric all-optical deflectors; bottom line: radially symmetric structures.

Periodic, quasi-periodic, and random quadratic nonlinear photonic crystals

Ady Arie [*] *and Noa Voloch*

Dept. of Physical Electronics, School of Electrical Engineering, Iby and Aladar Fleischman Faculty of Engineering, Tel-Aviv University, Tel-Aviv 69978, Israel

1. Introduction

When an electromagnetic field of angular frequency ω travels through a dielectric medium, it induces electrical dipoles in the material's atoms. These dipoles usually oscillate in the same angular frequency ω as that of the forcing electromagenetic field. The macroscopic induced dipole moment per unit volume is the material polarization $\mathbf{P}(\omega)$, and it is related to the electric field by the linear electrical susceptibility $\chi^{(1)}(\omega)$. The real and imaginary part of the linear susceptibility determine the material's dispersion and absorption. The absorption occurs since the electromagnetic wave transfers energy to the atoms by inducing oscillating dipoles. However, the energy can also flow from the atoms to the electromagnetic field, since the oscillating dipoles are small antennas that radiate electromagenetic waves. The electric field may also induce dipoles in the material that oscillate in integer multiples of ω. Far from resonance, the induced polarization can be written as a Taylor expansion: $\mathbf{P} = \epsilon_0 \left[\chi^{(1)}\mathbf{E} + \chi^{(2)}\mathbf{E^2} + \chi^{(3)}\mathbf{E^3} + \ldots \right]$, where ϵ_0 is the vacuum permittivity and $\chi^{(2)}, \chi^{(3)}$ are the second and third order electrical susceptibility. The electric field and polarization are three-dimensional vectors, hence $\chi^{(1)}, \chi^{(2)}, \chi^{(3)}$ are $3 \times 3, 3 \times 3 \times 3$ and $3 \times 3 \times 3 \times 3$ ten-

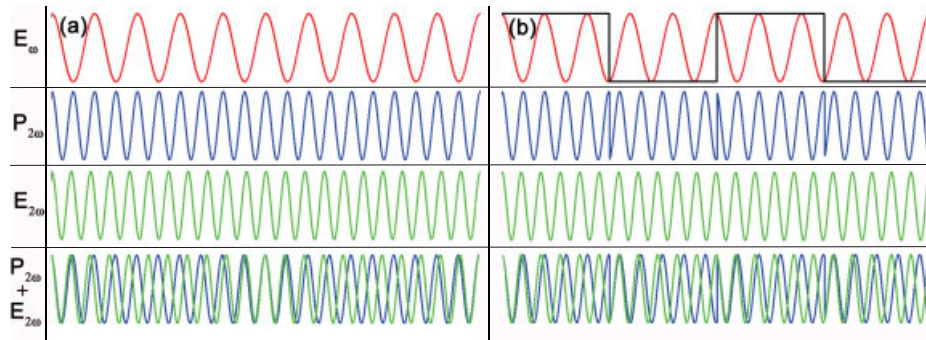[*] Corresponding author: e-mail: ady@eng.tau.ac.il

Figure 1 (online color at: www.lpr-journal.org) Electric field at ω, induced polarization at 2ω, electric field at 2ω and combined polarization and second harmonic field: (a) Homogeneous crystal. Owing to dispersion, the induced polarization becomes out of phase with the electric field that was generated at the beginning of the crystal. (b) Periodic reversal of the material nonlinear coefficient brings the polarization back in phase with the second harmonic wave.

sors. Here we consider for simplicity one component of the induced polarization, and assume that we can select a single component from each one of the three tensors to relate between the electric fields and the polarization component.

The first nonlinear term, $\epsilon_0 \chi^{(2)} E^2$, scales as the square of the electromagnetic field. This so-called quadratic nonlinearity is responsible for various three-wave mixing processes, in which waves at frequencies ω_1, ω_2 generate waves at new frequencies $\omega_3 = 2\omega_1$, $2\omega_2$, $\omega_1 \pm \omega_2$ and 0. It should be noted that for many materials the second order susceptibility $\chi^{(2)}$ is zero, and therefore the strongest nonlinearity is cubic, governed by $\chi^{(3)}$. The quadratic nonlinearity is non-zero only in a small group of materials that lack inversion symmetry center, and are called non-centrosymmetric materials.

Let us consider as an example the special and important process of second harmonic generation, in which a wave of angular frequency ω generates a new waves of angular frequency 2ω. The nonlinear effect is usually a weak effect, and in order to obtain sufficient conversion efficiency, the nonlinear device should therefore be much longer than the wavelength. The typical length is in the cm range, 4 orders of magnitude longer than the typical optical wavelength. Ideally, second harmonic waves that were generated in different parts of the nonlinear crystal will interfere constructively. However, the induced polarization depends on the wave-vector $\mathbf{k}(\omega)$ (and hence of the refractive index $n(\omega)$) of the generating waves, whereas the propagation of the nonlinearly generated wave depends on $\mathbf{k}(2\omega)$ (hence on $n(2\omega)$), as shown in Fig. 1. Unfortunately, owing to material dispersion, the refractive indices are different, and as a result light waves from different parts of the crystal will be out of phase and will therefore interfere destructively, resulting in a very small conversion efficiency. This so-called phase-matching problem is a key problem in quadratic nonlinear processes.

Various methods have been developed to overcome the phase matching problem. The most widely used method relies on the birefringence of the crystal. The key idea is to overcome dispersion by appropriate selection of the polar-
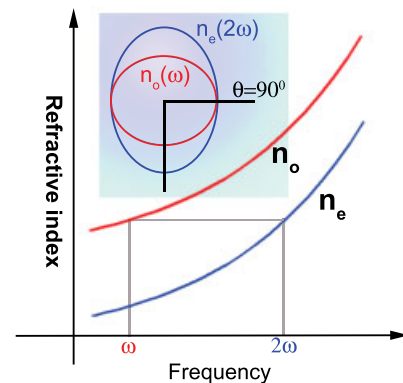

Figure 2 (online color at: www.lpr-journal.org) Typical dispersion curves for the ordinary and extraordinary refractive indices of a uniaxial crystal. Birefringent phase matching is achieved if $n_o(\omega) = n_e(2\omega)$ Inset shows the index ellipse of the ordinary wave at ω (which is a circle) and the extraordinary wave at 2ω.

izations of the interacting waves. As an example, in Fig. 2 we show the dispersion curves of the ordinary and extraordinary polarizations in a uniaxial material. As can be seen, for a certain angular frequency ω we get $n_o(\omega) = n_e(2\omega)$. The nonlinear polarization term that generates the second harmonic is proportional to the product of $\chi^{(2)}_{zxx}$ and the square of the x-component of the electric field at angular frequency ω. However, birefringent phase matching suffers from several drawbacks: (a) It is not always possible to compensate the material's dispersion. For example, second harmonic generation cannot be birefringently phase-matched in LiNbO$_3$ for generating wavelengths in the blue and ultraviolet ranges. (b) One is limited to the use of non-diagonal terms of the $\chi^{(2)}$ tensor, but the stronger components are the diagonal components. For example, in LiNbO$_3$, $\chi^{(2)}_{zzz}$ is approximately seven times larger than $\chi^{(2)}_{zxx}$. However, to use this diagonal term, all the three interacting waves must be extra-ordinary polarized, and in this case one cannot rely on the crystal's birefringence to compensate the dispersion.
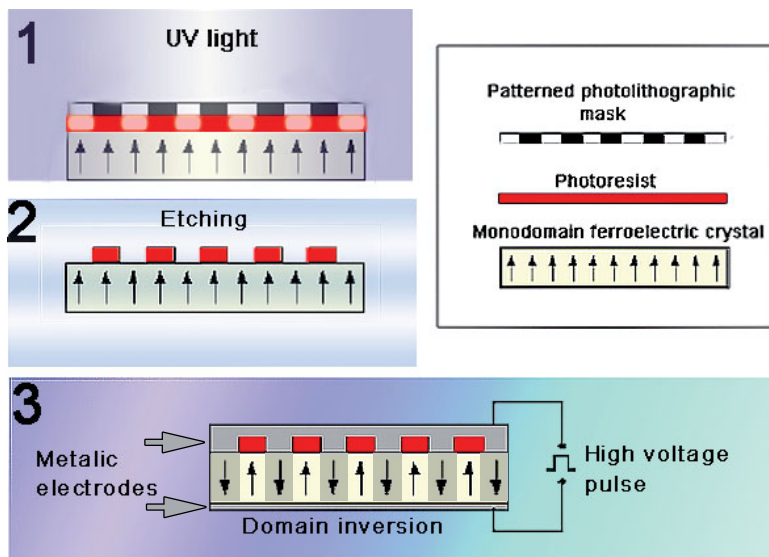
Figure 3 (online color at: www.lpr-journal.org) Electric field poling technique: 1) Photolithography of a photoresist-coated ferroelectric crystal. 2) Etching of exposed areas in the photoresist. The top and bottom surfaces of the crystal are then coated with electrodes. 3) A high voltage pulse reverses the sign of the electrical dipoles in areas in which the top metal is in contact with the crystal.

A second method to solve the phase matching problem is to spatially modulate the nonlinear coefficient as illustrated in Fig. 1b. This method is called quasi-phase matching [1, 2] (QPM) and in its simplest form is just a periodic binary modulation at a fixed spatial frequency. It allows to phase match any nonlinear process in the transparency range of the mixing crystal by choosing an appropriate modulation frequency. Moreover, the process can be done with any chosen nonlinear coefficient and in particular with the diagonal terms of the $\chi^{(2)}$ tensor. Perhaps the most interesting possibility enabled by quasi phase matching is the ability to shape the spectral and temporal response of the nonlinear mixer. This method has its own disadvantages:

(a) The modulation of the nonlinear coefficient reduces the efficiency. As an example, a binary periodic modulation reduces the conversion efficiency by a factor of at least $(2/\pi)^2 \approx 0.4$

(b) A suitable method is needed for modulating the nonlinear coefficient, and with adequate spatial resolution.

Fortunately, there was a significant progress in development of methods to modulate the nonlinear coefficient in the last decade. In particular, the electric field poling method [3] has been used successfully to pole various ferroelectric crystal such as LiNbO$_3$, LiTaO$_3$, KTiOPOtsb4, etc. The method relies on applying a high voltage pulse through a patterned electrode, as shown in Fig. 3. If the applied field surpasses the coercive field of the ferroelectric crystal, the direction of the electrical dipole is reversed in areas defined by the electrodes. In these materials, the required poling resolutions are typically in the 5–10 μm range for interactions in the visible and near infrared, and 20–40 μm for interactions in the mid-infrared.

Periodically-poled ferroelectric crystals with these periods are now commercially available from several vendors. Sub-micron resolutions [4, 5] have been reached in research laboratories for special non-collinear and backward nonlinear interactions.

Another promising method for modulating the nonlinear coefficient is orientation patterning of semiconductors such as GaAs [6]. GaAs is particularly attractive in the mid-infrared range, owing to its high transparency in the range 1–16 μm (whereas most ferroelectric materials have excellent transmission in the visible and near infrared, but are almost opaque for wavelengths above 5 μm). GaAs also has a very high nonlinear coefficient $d_{14} \approx 100 \frac{pm}{V}$ (3–5 times higher than the highest nonlinear coefficient of ferroelectrics), excellent mechanical properties and high thermal conductivity. GaAs is optically isotropic, therefore it cannot be birefringently phase matched. However, QPM is possible in samples in which the crystallographic orientation (and hence the sign of d_{14}) is periodically rotated. The period is set by defining a thin periodic Ge buffer layer on GaAs substrate, followed by epitaxial growth of layers with different orientations of the GaAs substrate and on the Ge layer, see Fig. 4. Hydride vapor phase epitaxy enables to reach samples with thickness of 500 μm, which is sufficiently thick for many nonlinear optical applications.
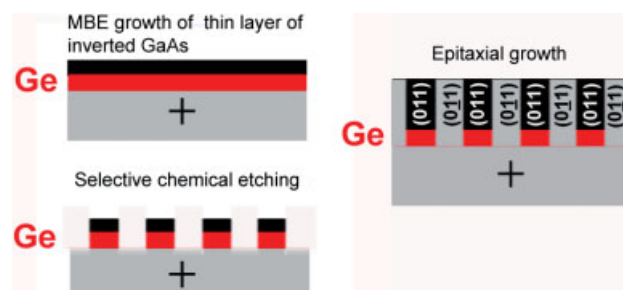

Figure 4 (online color at: www.lpr-journal.org) Fabrication process for orientation patterned GaAs: A Ge buffer layer is grown on a GaAs substrate, followed by selective chemical etching and epitaxial growth. The orientation of the GaAs that grows on the Ge buffer layer is rotated with respect to that of the buffer layer.
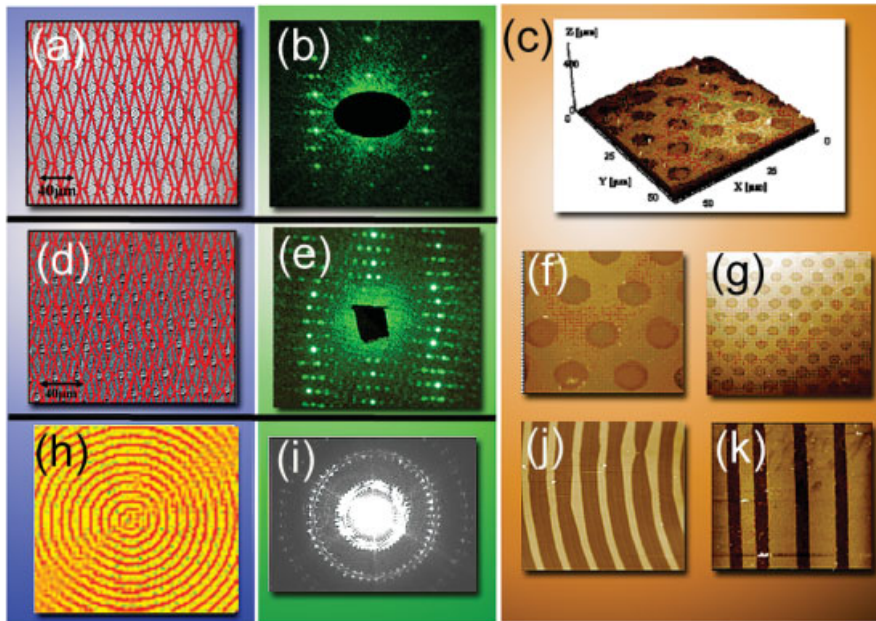
Figure 5 (online color at: www.lpr-journal.org) Examples of nonlinear photonic crystals. (a,d) are optical microscope images of the top views of two-dimensional quasi-periodic structures embedded with the underlying quasi-periodic lattices (the SHG Fan and the Frequency Fan, see Sect. 4 for details). (h) is the image of annular periodic nonlinear photonic crystals. (b,e), and (i) are the corresponding far field diffraction patterns of the three NLPCs. (c,f), and (g) are atomic force microscope (AFM) images of two-dimensiona periodic NLPC having hexagonal lattice and circular motif. (j) is an AFM image of the annular NLPC and (k) is an AFM image of a 1D quasi-periodic NLPC.

Other methods include poling of ferroelectrics by ion-exchange or electron beam irradiation [2, 7], optical and electrical poling of polymers [8] and electrical poling of glasses [9, 10]. For the ferroelectric or semiconductors materials the nonlinear coefficient is alternating between a positive and negative value, whereas for glasses and polymers the nonlinear coefficient alters between a non-zero value in the poled regions and null nonlinearity in the remaining parts.

The modulation of the nonlinear coefficient can be more sophisticated than a simple one-dimensional periodic modulation, which is usually suitable for phase matching only a single nonlinear interactions. Additional degrees of freedom may be provided by using quasi-periodic [11–13] or even random [14, 15] modulation of the nonlinear coefficient. Another extension is provided by modulating the nonlinear coefficient in either two [16–18] or even three dimensions [19]. These possibilities enable to phase match multiple interactions, in different propagation directions of the input and output waves. Some examples of nonlinear structures are shown in Fig. 5.

Materials in which the second order susceptibility $\chi^{(2)}$ is spatially modulated, either periodically or a-periodically, while the linear susceptibility remains constant are called nonlinear photonic crystals (NLPCs). Since the linear susceptibility and correspondingly the refractive index are not altered, the NLPCs are significantly different than the more common photonic crystals, in which the linear susceptibility is modulated. It should be emphasized that other types of nonlinear interactions are possible in photonic crystals, including third-order ($\chi^{(3)}$) nonlinearities in "standard" photonic crystals [20, 21]. Furthermore, one dimensional photonic crystals in which both the linear and the second-order nonlinear susceptibilities are modulated have been analyzed [2, 22, 23]. Two dimensional and three dimensional

photonic crystals with modulated second order nonlinearity were reviewed in [24]. However, since the common techniques for modulating the second order nonlinearity (e.g. electric field poling in ferroelectric crystals, orientation patterning of semiconductors) do not alter the linear refractive index of the material, we will concentrate in this paper only on materials having homogeneous linear index and space-dependent second order nonlinear index.

In the following sections we shall analyze nonlinear interactions in NLPCs. The coupled wave equations in a material with either homogeneous or periodically modulated nonlinear coefficient will be presented in Sect. 2. In Sects. 3, 4, and 5 we shall consider interactions in more sophisticated NLPCs such as periodic two-dimensional NLPCs, quasi-periodic NLPCs and random NLPCs , respectively. Sect. 6 introduces some new types of NLPCs, e.g. NLPCs that are not lattice -based and posses radial symmetry, or special NLPCs that enable nonlinear beam deflection and beam transformation. Finally, Sect. 7 presents a summary and outlook for future developments in this field.

2. Wave equations in NLPC

Consider now the case of second harmonic generation in a NLPC. The results shown here can be easily generalized to other three wave mixing processes, e.g. sum frequency generation and difference frequency generation. Assuming that a plane wave of frequency ω propagates in the transverse plane of the NLPC, this wave generates a second harmonic wave owing to the second order susceptibility of the material. Assuming that the fundamental frequency is linearly polarized along one of the NLPC axes, and considering a specific linear polarization of the generated second harmonic wave, the coupling between the two beams is
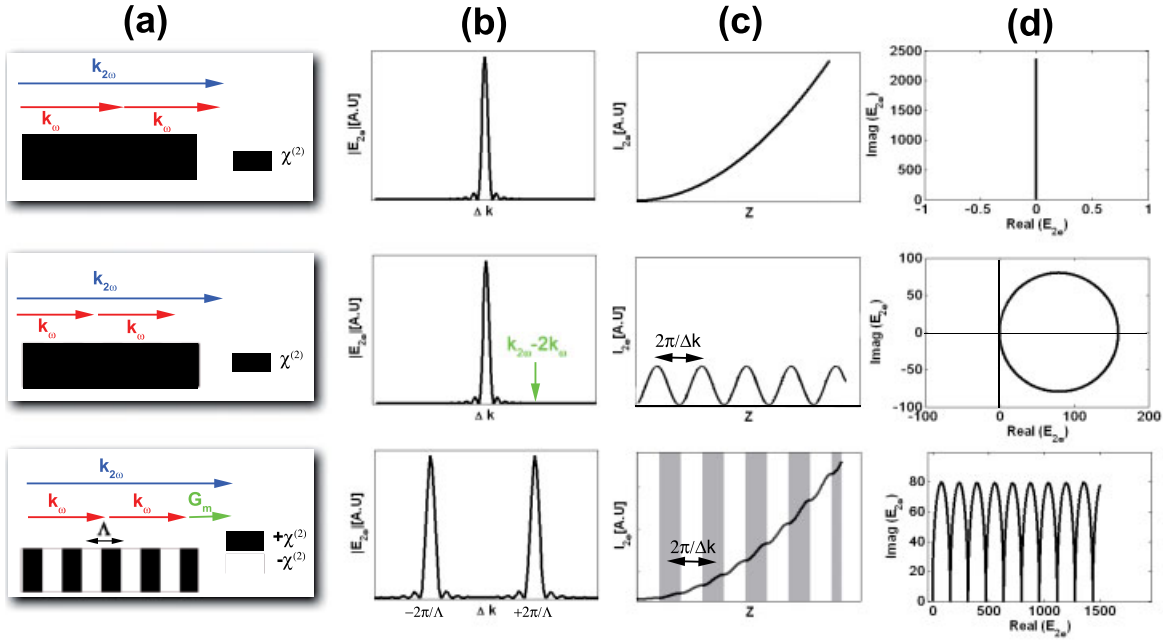
Figure 6 (online color at: www.lpr-journal.org) Phase matched, non-phase matched and (1D periodic) quasi-phase matched cases. From left to right: (a) Nonlinearity along the crystal and k-vector scheme, (b) Absolute value of the second harmonic field vs. the spatial frequency (c) Evolution of the second harmonic intensity along the crystal (d) Phasor diagram of the second harmonic wave .

given by the appropriate element of the nonlinear susceptibility tensor $d_{ij} = \chi_{ij}^{(2)}/2$, where i and j are contracted Cartesian indices [25].

The relevant components of the fundamental and second harmonic wave can be written as

$$\tilde{E}_\omega(\mathbf{r}, t) = \tfrac{1}{2} E_\omega(\mathbf{r}) \exp[i(\omega t - \mathbf{k}_\omega \cdot \mathbf{r})] + \text{c.c.}, \quad (1)$$

$$\tilde{E}_{2\omega}(\mathbf{r}, t) = \tfrac{1}{2} E_{2\omega}(\mathbf{r}) \exp[i(2\omega t - \mathbf{k}_{2\omega} \cdot \mathbf{r})] + \text{c.c.}, \quad (2)$$

Let us assume that the relative change of the field envelopes E_ω, $E_{2\omega}$ over a propagation distance of a wavelength is small. Under this so called slowly varying envelope approximation [25], the amplitudes of the fundamental and second harmonic waves are coupled by the nonlinear polarization (in M.K.S):

$$\mathbf{k}_\omega \cdot \nabla E_\omega(\mathbf{r}) = -i\frac{\omega^2}{c^2} E_{2\omega} E_\omega^* d_{ij}(\mathbf{r})$$
$$\times \exp[-i(\mathbf{k}_{2\omega} - 2\mathbf{k}_\omega) \cdot \mathbf{r}], \quad (3)$$

$$\mathbf{k}_{2\omega} \cdot \nabla E_{2\omega}(\mathbf{r}) = -2i\frac{\omega^2}{c^2} E_\omega^2 d_{ij}(\mathbf{r})$$
$$\times \exp[i(\mathbf{k}_{2\omega} - 2\mathbf{k}_\omega) \cdot \mathbf{r}], \quad (4)$$

where E_ω^* is the complex conjugate of E_ω. Assuming that the nonlinear conversion efficiency is low, the pump amplitude can be assumed constant throughout the entire interaction length (non-depletion approximation). In this case, we consider only the evolution of the second harmonic field. Let us examine this equation in a particular case in which

both the fundamental and second harmonic waves propagate along the Z direction. We shall also assume that the modulation of the nonlinear coefficient is only along the Z direction. In this case, the wave equation for the second harmonic wave has a simpler, scalar form:

$$\frac{dE_{2\omega}(z)}{dz} = -i\frac{\omega}{n_{2\omega}c} E_\omega^2 d_{ij}(z) \exp[i(k_{2\omega} - 2k_\omega)z]. \quad (5)$$

For a crystal of length L, the second harmonic field is therefore given by:

$$E_{2\omega}(L) = -i\frac{\omega}{n_{2\omega}c} E_\omega^2 \int_{-\infty}^{\infty} d_{ij}(z) \exp(i\Delta k z) dz, \quad (6)$$

where $\Delta k \equiv k_{2\omega} - 2k_\omega$ is the phase mismatch. Note that the integral is peformed from $-\infty$ to ∞ by extending the definition the nonlinear function $d_{ij}(z)$ for every z, equating it to zero outside the crystal. This equation shows that the electric field at the end of the crystal is proportional to the Fourier transform of the space-dependent nonlinearity. It is convenient to define the nonlinearity as the product of a fixed value of the nonlinear tensor d_{ij} and a unilitess space dependent function $g(z)$. The electric field at the end of the crystal is therefore proportional to its Fourier transform

$$G(\Delta k) = \frac{1}{L} \int_{-\infty}^{\infty} g(z) \exp(i\Delta k z) dz. \quad (7)$$

In the next sections and in Fig. 6 we examine three important cases – perfect phase matching, no phase matching and periodic 1D quasi phase matching.

(a) Perfect phase matched case in an homogeneous crystal, where $\Delta k = 0$. Here we have a monotonous linear (quadratic) buildup of the second harmonic amplitude (intensity). In this case we get $G(0) = 1, E_{2\omega}(L) = -i\frac{\omega d_{ij} L}{n_{2\omega} c} E_\omega^2$ and

$$I_{2\omega} = \frac{2\omega^2 d_{ij}^2}{n_{2\omega} n_\omega^2 c^3 \varepsilon_0} I_\omega^2 L^2, \tag{8}$$

where we have used the relation $I = nc\epsilon_0 E^2/2$.

(b) Non-phase matched case in an homogeneous crystal, where $\Delta k \neq 0$. In this case, using Eqs. (6) and (7) one obtains

$$E_{2\omega}(L) = -\frac{\omega d_{ij}}{n_{2\omega} c} E_\omega^2 \frac{e^{i\Delta k L} - 1}{\Delta k}, \tag{9}$$

$$I_{2\omega} = \frac{2\omega^2 d_{ij}^2}{n_{2\omega} n_\omega^2 c^3 \varepsilon_0} I_\omega^2 L^2 \frac{\sin^2(\Delta k L/2)}{(\Delta k L/2)^2}$$

$$= \frac{8\omega^2 d_{ij}^2}{n_{2\omega} n_\omega^2 \Delta k^2 c^3 \varepsilon_0} I_\omega^2 \sin^2(\Delta k L/2). \tag{10}$$

If Δk is less than π/L then there is still a reasonable efficiency, however for larger phase mismatch values, we get a rapidly oscillating term in Eq. (6), which results in negligible conversion efficiency. The second harmonic amplitude oscillates with a characteristic length $L_c = \pi/\Delta k$.

(c) Quasi phase matched case in a periodically modulated crystal. Here the phase mismatch is balanced by the modulation of the nonlinear coefficient. Let us consider a periodic modulation with a period Λ, where the lengths of the positive and negative nonlinear coefficient in each period is equal. In this case the nonlinear function can be described by

$$d(z) = \begin{cases} \text{sign}\left[\cos\left(\frac{2\pi z}{\Lambda}\right)\right], & -L/2 \leq z \leq L/2 \\ 0, & \text{otherwise} \end{cases} \tag{11}$$

In the case of an infinitely long crystal, the nonlinear coefficient can be written as a Fourier series

$$d(z) = \sum_{m=-\infty}^{m=\infty} G_m \exp(-iK_m z), \tag{12}$$

where is $G_m = \frac{2}{\pi m} \sin(\frac{\pi m}{2})$ and $K_m = \frac{2\pi m}{\Lambda}$. Note that the Fourier coefficient G_m is non-zero only for the odd values of m. Quasi phase matching occurs when $K_m = \Delta k$, or more explicitly:

$$\frac{2\pi m}{\Lambda} = k_{2\omega} - 2k_\omega. \tag{13}$$

If we insert the Fourier decomposition expression of Eq. (12) in Eq. (6), it is easy to see that for all the non-phase matched components of the Fourier series, one gets

an oscillating term whose integral is nearly zero. Only the phase matched term will lead to a significant build-up of the second harmonic power:

$$E_{2\omega}(L) \approx -i\frac{\omega d_{ij} G_m L}{n_{2\omega} c} E_\omega^2. \tag{14}$$

The second harmonic intensity in this case is

$$I_{2\omega} \approx \frac{2\omega^2 d_{ij}^2 |G_m|^2}{n_{2\omega} n_\omega^2 c^3 \varepsilon_0} I_\omega^2 L^2. \tag{15}$$

By comparing Eq. (15) to Eq. (8), we see that the quasi phase matched field (intensity) is smaller by a factor of G_m ($|G_m|^2$) with respect to the perfectly phase-matched case. The largest Fourier coefficient is $G_1 = \frac{2}{\pi} \approx 0.64$. However, in quasi-phase matching one can use the (relatively large) diagonal elements of the $\chi^{(2)}$ tensor, which cannot be used in birefringent phase matching, hence the total efficiency can be larger for QPM. For example, in LiNbO$_3$ we have $(2/\pi)d_{33} \approx 3.8 d_{31}$, therefore, the intensity conversion efficiency can be $3.8^2 \approx 14.4$ times higher for QPM interactions.

A more general case of periodic one dimensional modulation occurs when the size of the positive and negative is not equal. We define the ratio of the (say) positive part to the period Λ as the duty cycle D. So far, we have considered only the case of $D = 0.5$, but this parameter can get any value between 0 and 1. The nonlinear coefficient in the general case can be represented by

$$d_{ij}(x) = d_{ij} \text{sign}\left[\text{saw}\left(\frac{x}{\Lambda} - D\right) - \text{saw}\left(\frac{x}{\Lambda}\right)\right]$$

$$= d_{ij} \sum_{m=-\infty}^{\infty} G_m e^{ik_m x}, \tag{16}$$

where saw is the saw-tooth function

$$\text{saw}(x) = 2\left[x - \text{floor}(x)\right] - 1.$$

In this case the Fourier coefficient is

$$G_m = 2\sin(m\pi D)/m\pi.$$

Note that the even orders of the Fourier decomposition may also be used now, provided $D \neq 0.5$. As an example, the highest values of the second Fourier coefficient, $G_2 = \frac{1}{\pi} \approx 0.318$, is obtained for $D = 0.25, 0.75$. The intensity conversion coefficient of second order QPM is 1/4 of a first order QPM (with optimal D of 0.5) and $\approx 1/10$ of perfect phase matching.

Although the higher QPM orders suffer from lower efficiency, owing to the smaller Fourier coefficients, they are sometimes used since for a given nonlinear process, the required period is proportional to the order. In cases in which the material exhibits high spectral dispersion, the required period in first order QPM may be smaller than the
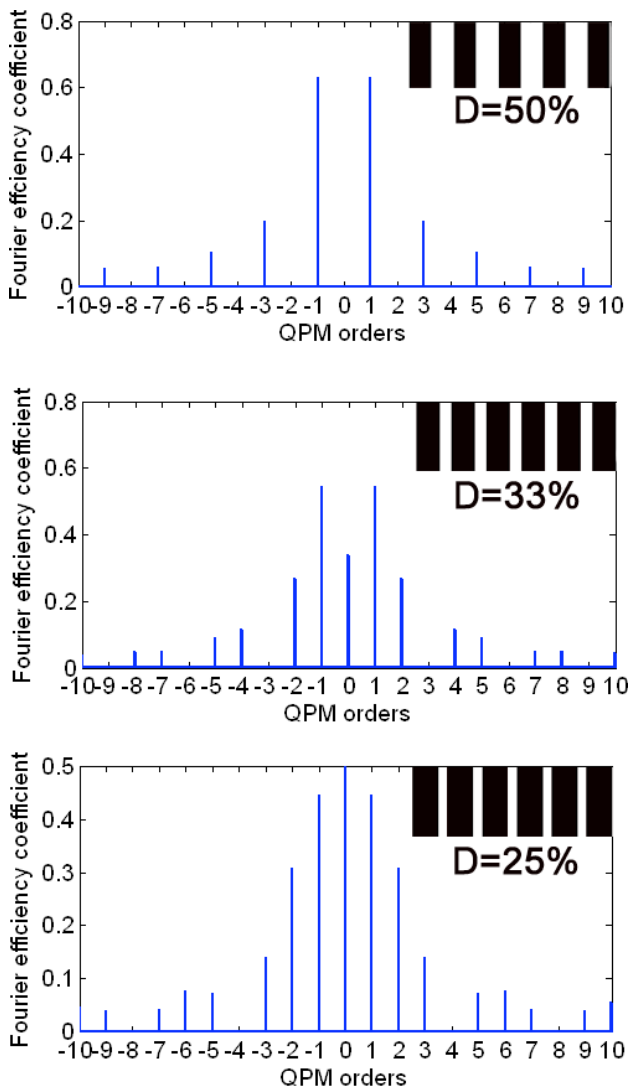
Figure 7 (online color at: www.lpr-journal.org) Absolute value of the Fourier coefficient $|G_m|$ as a function of the QPM order m for different duty cycles D (a) D=0.5, (b) D=0.33 (c) D=0.25

resolution of the nonlinear modulation. In these cases, a higher QPM order is very useful. One precaution is that higher QPM orders require tighter control of the fabricated duty cycle. In Fig. 7 we show the absolute value of the Fourier coefficient $|G_m|$ as a function of the QPM order m for duty cycles of 0.5, 0.33 and 0.25. As can be seen, the efficiency of the second order QPM is nullified for $D = 0.5$, while the third order QPM efficiency is nullified for $D = \frac{1}{3}$ (and also for $D = \frac{2}{3}$).

So far, we have considered only quasi phase matching in infinitely long crystals. For a real crystal with finite length L, we need to multiply the infinitely long nonlinear function of Eq. (16) with the rectangle function $\mathrm{rect}\,(z/L)$ (which is unity when the absolute value of the argument is less than 1/2 and 0 otherwise). In the Fourier space, this will lead to a convolution of the Fourier transform of Eq. (16) (which is a

series of delta functions at $\frac{2\pi m}{\Lambda}$) with the Fourier transform of the rectangle function, i.e. $\frac{\sin(\Delta k L/2)}{k L/2}$. As in the case of the homogeneous crystal, the finite crystal length provides some tolerance in the phase mismatch, i.e. for a given QPM order m, the process is still relatively efficient provided that $\Delta k_{\mathrm{QPM}} = k_{2\omega} - 2k_\omega - \frac{2\pi m}{\Lambda} < \pi/L$. If only this order dominates, and for all other QPM orders the phase mismatch is so large that their contribution is negligible, we can derive the second harmonic intensity:

$$I_{2\omega} \approx \frac{2\omega^2 d_{ij}^2 |G_m|^2}{n_{2\omega} n_\omega^2 c^3 \varepsilon_0} I_\omega^2 L^2 \frac{\sin^2(\Delta k_{\mathrm{QPM}} L/2)}{(\Delta k_{\mathrm{QPM}} L/2)^2} \,. \quad (17)$$

3. Periodic two-dimensional nonlinear photonic crystals

Berger [16] proposed in 1998 to extend the concept of periodic quasi-phase matching from one-dimension to two-dimensions. This immediately increases the flexibility of the nonlinear devices, and allows to phase match several different processes in different directions. Moreover, since the techniques to modulate the nonlinear coefficient, e.g electric field poling, are in any case planar techniques, the experimental realization of 2D-modulated devices is straightforward. The first experimental realization was made by Broderick et al. [17]. Some recent examples include simultaneous wavelength interchange [26], third and fourth harmonic generation [27, 28], and proposed realization of all optical effects, e.g. all optical deflection and splitting [29].

The analysis of both one and two-dimensional NLPCs can be modeled as a convolution between a periodic lattice and a nonlinear motif, as shown in the two examples of Fig. 8. In the case of a 1D structure, the lattice is a set of equally spaced points (their distance is the lattice period Λ), and the motif is a strip having a nonlinear coefficient with a different sign than the background. Likewise, a 2D NLPC is obtained by convolving a 2D lattice with a nonlinear motif. The two-dimensional lattice is defined by two primitive, non-parallel vectors $\mathbf{a}_1$ and $\mathbf{a}_2$, and the lattice points are given by $\mathbf{r}_{mn} = m\mathbf{a}_1 + n\mathbf{a}_2$. The motif is some two dimensional geometrical shape, e.g., circle, hexagon, rectangle etc., having a nonlinear coefficient that is different that the background. The pattern outside the motifs, may be linear (zero nonlinearity, as for example is the case for patterns made of poled and un-poled glass), or may have an opposite sign of the nonlinear coefficient in the case of domain inverted ferroelectric crystals). If the background is nonlinear (with opposite sign to the motif nonlinear coefficient) the motif function denoted $s(\mathbf{r})$, has values of 1 and (-1) instead of 1 and 0. This amount in a DC shift in the Fourier transform of the overall structure function. The result, as implied through Eq. (14) in Sec. 2 , is doubling of the electric field conversion efficiency for a QPM process. To simplify the following analysis we assume that the background has a zero nonlinear coefficient, while later the final results are adjusted to account for non-zero background. In
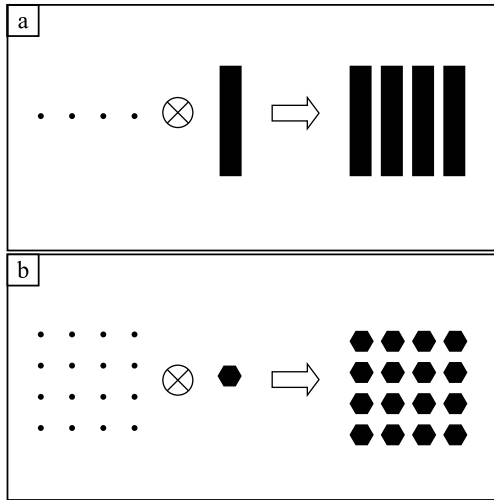
Figure 8 Examples of convolution for NLPC: (a) 1D lattice, (b) a square 2D lattice with hexagonal motif.
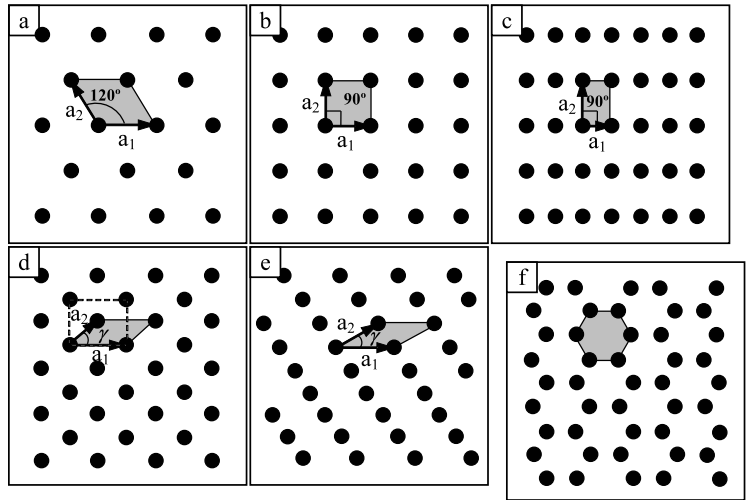

Figure 9 The six lattice types, five of them (a–e) are Bravais lattices: (a) hexagonal, (b) square, (c) rectangular, (d) centered-rectangular, where the dashed lines form a rectangle, (e) oblique. Panel (f) is a honeycomb lattice. The gray area in each one of the lattices refers to its unit cell.

addition, we assume that the lattice area is restricted by a rectangular interaction area $a(\mathbf{r})$.

The 2D periodic structures [30] can be classified by five Bravais lattices: Hexagonal, square, rectangular, centered rectangular and oblique, as can be seen in Figs. 9a–e. Note that in the photonic crystals community, the hexagonal lattice is identified as a "triangular" lattice, while "hexagonal" or "honey-comb" lattice (in this community) is actually a hexagonal lattice with a missing point in the middle of each hexagon (see Fig. 9f).

As in the case of 1D NLPC, the nonlinearity as a function of space in an infinite 2D periodic structure can also be written by a Fourier series:

$$d_{ij}(\mathbf{r}) = d_{ij}\sum G_{mn}\exp(-i\mathbf{K}_{mn}\cdot\mathbf{r}) = d_{ij}g(\mathbf{r}),\ (18)$$

where $g(\mathbf{r})$ is a normalized and dimensionless function, representing the space dependence of the nonlinear coefficient function. $\mathbf{K}_{mn}$ are vectors in the reciprocal lattice [30], defined by two primitive vectors that are orthogonal to the real lattice primitive vectors, i.e.

$$\mathbf{a}_i\cdot\mathbf{b}_j = 2\pi\delta_{ij},\ (19)$$

The 2D reciprocal lattice points are given by

$$\mathbf{K}_{mn} = m\mathbf{b}_1 + n\mathbf{b}_2.\ (20)$$

Significant build-up of the second harmonic wave requires phase matching, i.e. $\mathbf{k}_{2\omega} - 2\mathbf{k}_\omega - \mathbf{K}_{mn} \approx 0$. As in the 1D case, the vectorial phase-matching condition is just a crystal-momentum conservation law: the required momentum balance for the interaction is accomplished through a reciprocal lattice vector (RLV). Usually it can be assumed that if the phase matching condition is achieved by some

order (m, n), it would be the only order which contributes to the build-up of the second harmonic while all the other orders contributes negligible oscillating terms. The analysis for two-dimensional periodic structures can now be continued by rewriting the wave Eq. (4) as:

$$\mathbf{k}_{2\omega}\cdot\nabla E_{2\omega}(\mathbf{r})\ (21)$$

$$= -2i\frac{\omega^2}{c^2}E_\omega^2 d_{ij}\cdot G_{mn}\exp[i(\mathbf{k}_{2\omega} - 2\mathbf{k}_\omega - \mathbf{K}_{mn})\cdot\mathbf{r}].$$

Similar to what we have done in the previous section for a 1D lattice, it is convenient to analyze this interaction in the Fourier space, by integrating (21) over a rectangular area $a(\mathbf{r})$ of length L and width W (see an example [31]). The result is the second harmonic amplitude after an interaction length of L:

$$E_{2\omega}(\Delta\mathbf{k}) = \frac{-2i\omega^2 E_\omega^2 d_{ij}}{k_{2\omega}c^2 W}\iint_{a(\mathbf{r})}g(\mathbf{r})\exp(-i\Delta\mathbf{k}\cdot\mathbf{r})\mathrm{da},$$
$$(22)$$

where $\Delta\mathbf{k} = \mathbf{k}_{2\omega} - 2\mathbf{k}_\omega$ is the phase-mismatch vector and $a(\mathbf{r}) = \mathrm{rect}(x/L)\cdot\mathrm{rect}(y/W)$ is the integration area. Setting $g(\mathbf{r})$ to zero outside the NLPC, the integration limits can be extended to infinity and so:

$$E_{2\omega}(\Delta\mathbf{k}) = \frac{-i\omega E_\omega^2 d_{ij}}{n_{2\omega}cW}G(\Delta\mathbf{k}),\ (23)$$

where $G(\Delta\mathbf{k})$ in this case is the two-dimensional Fourier transform of $g(\mathbf{r})$. From (23) it can be seen that the amplitude of the second harmonic wave for a specific phase mismatch value $\Delta\mathbf{k} = \Delta\mathbf{k}_0$ is proportional to $|G(\Delta\mathbf{k}_0)|$.

Let us assume that for the (m, n) order we reach perfect phase matching, $\Delta\mathbf{k}_{mn} = \Delta\mathbf{k} - \mathbf{K}_{mn} = 0$. In this case, it

is easy to calculate the second harmonic intensity after an interaction length L:

$$I_{2\omega} \approx \frac{2\omega^2 d_{ij}^2 |G_{mn}|^2}{n_{2\omega} n_\omega^2 c^3 \varepsilon_0} I_\omega^2 L^2, \qquad (24)$$

Hence, the interaction efficiency is proportional to the absolute square of the relevant Fourier coefficient $|G_{mn}|^2$. Note that this is almost identical to the expression in 1D NLPC, in Eq. (15), and the only difference is that the 1D Fourier coefficient $|G_m|^2$ is replaced by the two dimensional coefficient, $|G_{mn}|^2$.

In the case of infinite area, $G(\mathbf{f})$ consists of a distributed set of Dirac delta functions (Bragg peaks), located at integral combinations of the reciprocal lattice base vectors. As shown in [18] the Fourier coefficient becomes

$$G_{mn} = \frac{1}{A_{\mathrm{UC}}} S\left(\frac{\mathbf{K}_{mn}}{2\pi}\right). \qquad (25)$$

where $A_{\mathrm{UC}} = |a_{1x} a_{2y} - a_{1y} a_{2x}|$ is the area of the unit cell [32], $\mathbf{a}_1 = (a_{1x}, a_{1y})$, $\mathbf{a}_2 = (a_{2x}, a_{2y})$ are the real lattice primitive vectors and S is the Fourier transform of the motif function. Eq. (25) shows the combined effect of the lattice (through the unit cell area), the motif (through its Fourier transform function S) and the QPM orders m, n on the nonlinear process. For some specific motif functions, $S(\mathbf{f})$ is known analytically.

The effect of the lattice and motif in 2D NLPC was studied in detail in [18] and [33]. All the six lattices shown in Fig. 9 were analyzed, with four possible types of motifs: circular, rectangular, triangle and hexagonal. To illustrate these effects, let us consider here an example of a circular motif, with three possible lattices: hexagonal, square and rectangular lattices. The circular motif and its Fourier transform are:

$$s(\mathbf{r}) = \mathrm{circ}\left(\frac{|\mathbf{r}|}{R}\right) \equiv \begin{cases} 1, & |\mathbf{r}| \leq R \\ 0, & \text{elsewhere} \end{cases}, \qquad (26)$$

$$S(\mathbf{f}) = \frac{R}{|\mathbf{f}|} J_1(2\pi R |\mathbf{f}|). \qquad (27)$$

Table 1 displays the Fourier coefficient for a circular motif for each one of the three lattice types. This enables to

determine the highest possible efficiency for a given structure and the required dimensions and shape of the motif. Furthermore, it allows determining motif shapes that will completely null the nonlinear conversion efficiency (which, for example, can be useful to nullify unwanted processes).

Note that the Fourier coefficients in Table 1 are suitable for the case in which the background has an opposite nonlinear coefficient with respect to that of the motif (as is the case for domain-inverted ferroelectrics). If the background has zero-nonlinearity, the Fourier coefficients shown in Table 1 should be multiplied by $1/2$. The effects of other motifs can be calculated in a similar way using (25). Specifically, a the effect of rectangular motif was analyzed in [18], while triangular and hexagonal motifs were analyzed in [33].

The normalized efficiency is examined in Fig. 10 and Fig. 11 as a function of the normalized radius R/a (the ratio between the circle radius (R) and a primitive vector length (a)) for two specific QPM orders: $(m, n) = (1, 0)$ and $(1, 1)$, in two out of the six lattice types, namely the hexagonal and square lattices.

The first QPM order, $(1, 0)$ is usually the most efficient process in a 2D nonlinear structure, however it relies on only one of the two primitive vectors. The second QPM order, $(1, 1)$ is usually the most efficient process that relies on both primitive vectors, although in some cases, the $(1, 2)$ order and the $(2, -1)$ order [18], can be more efficient.

In the following analysis for each one of the different lattices, the motif size is limited in order to avoid overlap between motifs of adjacent lattice points, therefore the normalized radii in Fig. 10 and Fig. 11 do not exceed 0.5. The insets in those figures simply show the 2D NLPC for specific R/a ratios and lattice, the black circles represent a certain sign of the nonlinear coefficient, whereas the white areas represent the opposite sign.

The square lattice can provide higher efficiency compared to an hexagonal lattice, when a specific motif size is chosen. Fig. 10 shows that for order $(m, n) = (1, 0)$, the square lattice with a motif size of $R/a = 0.383$, provides the optimum efficiency $|G_{10}|^2 = 0.158$. A higher efficiency can be achieved in a rectangular lattice with two specific primitive vectors [18], whereas lower efficiency is obtained for the hexagonal lattice. For the order $(m, n) = (1, 1)$, the maximum efficiency $|G_{11}|^2 = 0.04$ is achieved for a square lattice with $R/a = 0.271$ (Fig. 11). For com-

Table 1 Fourier coefficient of a circular motif

Lattice types	Fourier coefficient G_{mn} of a circular motif
Hexagonal	$G_{mn}^{\mathrm{hex}} = \dfrac{2R}{a\sqrt{m^2 + n^2 + mn}} J_1\left(\dfrac{4\pi R}{a\sqrt{3}}\sqrt{m^2 + n^2 + mn}\right)$
Square	$G_{mn}^{\mathrm{sq}} = \dfrac{2R}{a\sqrt{m^2 + n^2}} J_1\left(\dfrac{2\pi R}{a}\sqrt{m^2 + n^2}\right)$
Rectangular	$G_{mn}^{\mathrm{rect}} = \dfrac{2R}{\sqrt{(ma_2)^2 + (na_1)^2}} J_1\left(2\pi R\sqrt{\dfrac{m^2}{a_1^2} + \dfrac{n^2}{a_2^2}}\right)$

Figure 10 Normalized efficiency for $(m, n) = (1, 0)$ order as a function of the motif radius to primitive vector magnitude ratio. The plus-sign, dashed and solid lines represent the efficiency curves for the hexagonal, square and honeycomb lattice, respectively. The inset shows the 2D NLPC for a square lattice with $R/a = 0.383$.
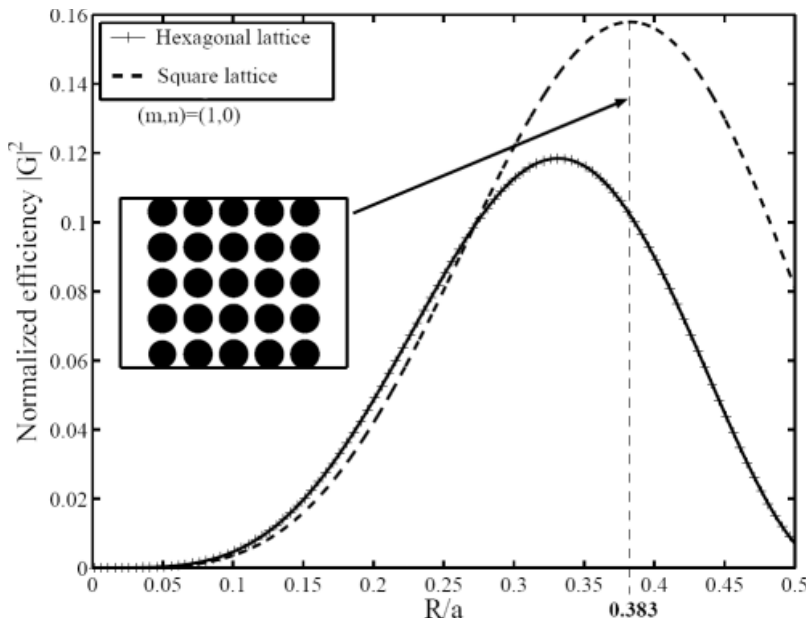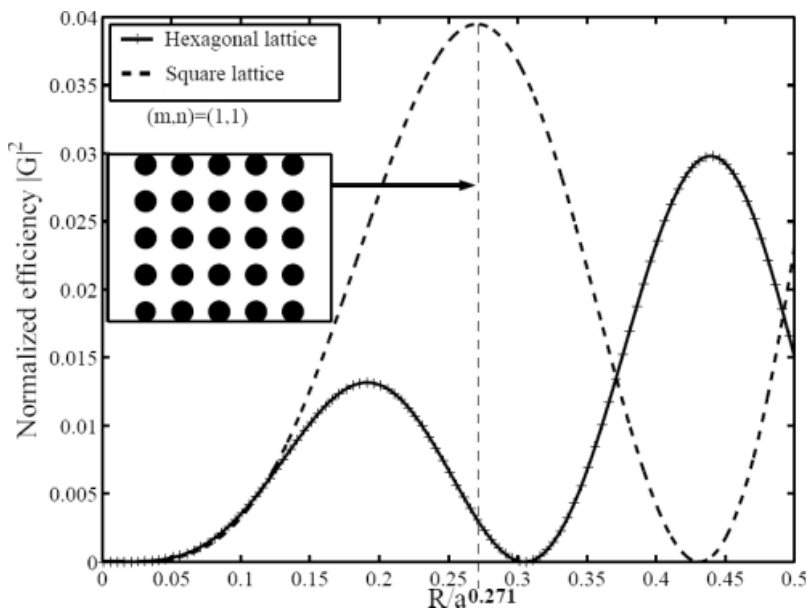

Figure 11 Normalized efficiency for $(m, n) = (1, 1)$ order as a function of the motif radius to primitive vector magnitude ratio. The plus-sign, dashed and solid lines represent the efficiency curves for the hexagonal, square and honeycomb lattice, respectively. The inset shows the 2D NLPC for a square lattice with $R/a = 0.271$.

parison, the highest efficiency of a periodic 1D structure is $|G_1(D = 0.5)|^2 = (2/\pi)^2 \simeq 0.4$.

The examples discussed in this section, are for normalized radii that provide high efficiencies. However, Table 1 and Figs. 10, 11 can also be used to extract normalized radii that nullify the conversion efficiency for specific orders and lattices.

4. Quasi-periodic nonlinear photonic crystal

One limitation of the nonlinear periodic structures is that they usually enable to phase match only processes whose mismatch vectors correspond to integer multiples of a single vector (in the 1D case) or to a vectorial sum of only two base vectors (in the 2D case). However, the modulation of the nonlinear susceptibility does not have to be periodic. Nevertheless, in some specific cases it can still be efficient and provide greater design flexibility for phase matching several different processes. For example, one can simultaneously quasi-phase-match two processes by non-collinear interactions in one-dimensional periodic structures [34]. Another method relies on multiplying the periodic structure with another periodic structure of different periodicity [35]. Since we can use only the positive or negative values of the nonlinear coefficient, the effect of this multiplication is periodic reversal in the phase of the higher-frequency periodic structure.
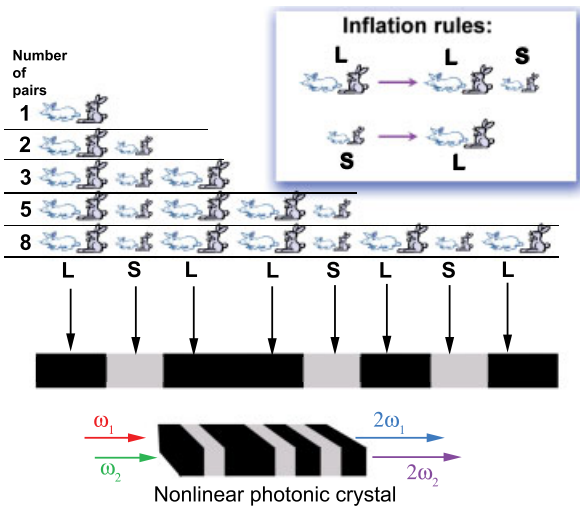
Figure 12 (online color at: www.lpr-journal.org) The way that rabbits breed was studied by Fibonacci in 1202. He assumed that they follow the inflation rule shown in the inset, i.e. in each cycle which takes one month, a mature pair can generate a new junior pair, whereas a junior pair become mature pair. The sequence of mature and junior pairs is a quasi-periodic sequence. It can be converted into a quasi-periodic nonlinear photonic crystal by replacing these pairs with long (L) and short (S) sections of modulated nonlinearity.

A general approach for simultaneous phase matching of different processes relies on quasi-periodic modulation of the nonlinear coefficient. Quasi-periodic structures are ordered structures that lack translation symmetry. Probably the first person to encounter quasi-periodicity was Fibonacci, who studied in 1202 the way that rabbits breed, see Fig. 12. Shechtman et al. [36] discovered quasi-periodic order in quasi-crystals, obtained by rapidly cooling of metallic alloys. Artificially grown (man-made) quasi-periodic superlattices were first obtained by Merlin et al. [37] through alternate growth of GaAs and AlAs layers by molecular beam epitaxy. Ming et al. [11] demonstrated the use of Fibonacci structures in nonlinear optics, e.g. for third harmonic generation. More general quasi-periodic modulations were studied in [12, 38, 39]. This concept was extended into two dimensions in [40, 41].

A general method to design frequency converters that will phase match any set of interacting waves, either in a 1D or in a 2D configuration, is provided by the so-called generalized Dual Grid Method (DGM) [42–44]. This method is well known in quasi-crystalline research, and is used for constructing tiling models of quasi-crystals. An important question that it addresses is how to design quasi-periodic structures under the constraint that the structure requirements in nonlinear optics are usually defined in the reciprocal (Fourier) space. Unlike for periodic NLPCs, there is no simple transformation between the reciprocal space and real space. The method that will be described here [13] provides a systematic method for designing the required nonlinear structure.

After selecting the nonlinear medium of choice and the appropriate operating temperature for a given frequency-conversion application, one can calculate the required set of mismatch vectors $\mathbf{\Delta k}^{(j)}$ $[j = 1, \ldots, N]$. The objective is to create an NLPC, represented geometrically by the normalized nonlinearity function $g(\mathbf{r})$, that will simultaneously phase match all processes. As was described in [13], once these mismatch vectors are known, one can use de-Bruijnís dual grid method [42], in order to design the required quasicrystal. If the N mismatch vectors are integrally-independent, one simply uses each vector $\mathbf{\Delta k}^{(j)}$ $[j = 1, \ldots, N]$ to define a family of equally-spaced parallel lines, separated by $\frac{2\pi}{\Delta k^{(j)}}$, and oriented in the direction of $\Delta k^{(j)}$. The set of all N families constitutes the dual grid, which is then used to define a set of N tiling vectors $a^{(j)}$, and to calculate the integral linear combinations of these tiling vectors that form the vertices of the tiles in the desired quasicrystal. The final step is to decorate each tile with an optimal motif, i.e. to decide which regions of the tile will be altered such that the relevant components of the quadratic dielectric tensor $\chi^{(2)}$ are positive, leaving the remaining background with an unchanged negative $\chi^{(2)}$. Let us demonstrate how this method is implemented in 1D and in 2D.

4.1. One-dimensional design of quasi-periodic NLPC

For the 1D case, let us assume that we need to simultaneously phase match two processes with phase mismatch values of Δk_1 and Δk_2, as illustrated in Fig. 13a. In this 1D case, the two mismatch vectors lie on the same line. We start by establishing an orthogonality condition in a space with dimensionality equal to the number of required mismatch vectors, two dimensional space in the present case. For this purpose, we consider the two one-dimensional mismatch vectors as a single vector containing two components: $\mathbf{k}_1 = (\Delta k^{(1)}, \Delta k^{(2)})$. This vector spans a one-dimensional subspace of a two dimensional vector space. With this vector an orthogonality relation needs to be defined in a two-dimensional space. For this purpose the newly formed vector is expanded into a 2×2 non-singular matrix by adding another vector, $\mathbf{q}_2$ orthogonal to the first, $\mathbf{q}_2 \cdot \mathbf{k}_1 = 0$, so that the newly formed matrix is:

$$\mathbf{K} = \begin{pmatrix} \Delta k^{(1)} & q_2^{(1)} \\ \Delta k^{(2)} & q_2^{(2)} \end{pmatrix} = \begin{pmatrix} \mathbf{K}^{(1)} \\ \mathbf{K}^{(2)} \end{pmatrix}. \quad (28)$$

Since we want to create a quasicrystal whose Fourier transform will support the mismatch vectors of the nonlinear processes, we require an orthogonality relation, similar to the one used for periodic lattices, but this time in a higher dimensional space. This relation is then projected into the subspace that contains the problem. The orthogonality condition we require is:

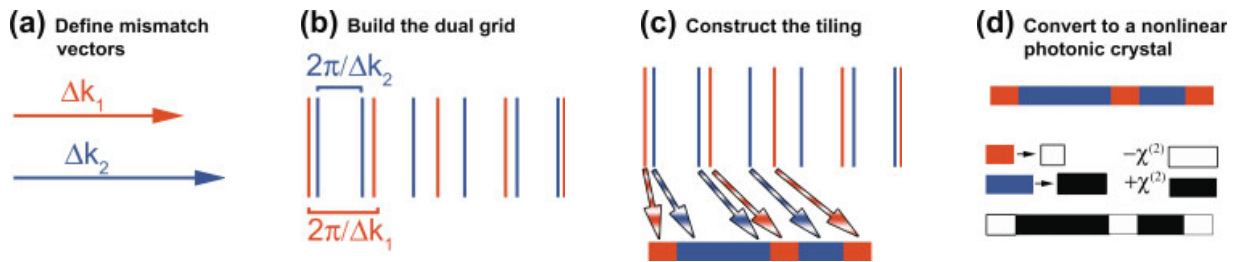$$\mathbf{A}^{(i)} \cdot \mathbf{K}^{(j)} = 2\pi \delta_{ij}. \quad (29)$$

Figure 13 (online color at: www.lpr-journal.org) Illustration of the solution for designing a one-dimensional NLPC for multiple collinear optical processes, using the dual grid method. In this example we show a design to phase match two processes. (a) The two required mismatch vectors. (b) The dual grid, in which each family of lines is shown with a different color. (c) Tiling of the real-space line according to the order in which lines of different families appear in the dual grid. (d) Associating a given duty cycle with each tiling vector (assumed to be with 100% or 0% in this example). Positively-poled segments are shown in black, and negatively-poled segments are shown in white.

Hence **A** is determined by:

$$\mathbf{A} = \begin{pmatrix} \mathbf{A}^{(1)} \\ \mathbf{A}^{(2)} \end{pmatrix} = 2\pi (\mathbf{K}^T)^{-1} . \tag{30}$$

The different components of the **A** matrix are denoted in the following way:

$$\mathbf{A} = \begin{pmatrix} a^{(1)} & b^{(1)} \\ a^{(2)} & b^{(2)} \end{pmatrix} . \tag{31}$$

$b^{(1)}$ and $b^{(2)}$ can be used to calculate the Fourier coefficients of every Bragg peak in the quasicrystal spectrum [13], whereas the $a^{(1)}$ and $a^{(2)}$ are used to span the quasi-periodic lattice using the dual grid construction. The dual grid is required in order to select only part of the points spanned by the base vectors of the quasi-crystal. If we would have taken all the points, the outcome would be dense filling of the space. Figs. 13b,c show how the dual grid method is used.

Once the real lattice is defined, we attach motifs representing the binary spatial modulation of the nonlinear photonic crystal. Each motif consists into two parts – one with $+\chi^{(2)}$ and the other with $-\chi^{(2)}$. Each such motif thus has a specific ratio or duty cycle (which in this case is the ratio of the length of the positive part to the tile spacing). The duty cycles of the different motifs can be used to optimize the efficiencies of the nonlinear processes. We have found out [45] that in many cases, the highest efficiencies are achieved when some of the motifs have 100% duty cycle while the others are with 0% duty cycle. These are also the easiest to fabricate structures in terms of required resolution. This is illustrated in Fig. 13d. In the designed structure the waves that are generated by the two processes will buildup, although sometimes not as smooth as in a periodic quasi-phase-matched structure, see Fig. 14. One interesting application that is enabled when two processes are collinearly phase matched is cross-polarization switching [46], where a type I second-harmonic-generation process $\omega_y + \omega_y \to 2\omega_y$ followed by a type II difference-
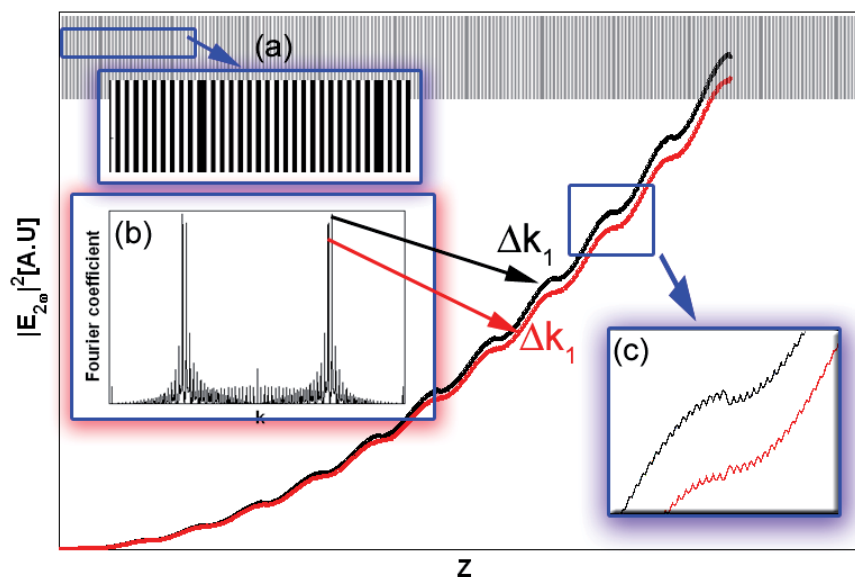

Figure 14 (online color at: www.lpr-journal.org) Evolution of the square absolute of the generated waves in a quasiperiodic nonlinear photonic crystal. Inset (a) is the nonlinear pattern as a function of crystal position; inset (b) is the absolute value of the Fourier transform $|G(\Delta k)|$; (c) is an expanded view of the square absolute of the two generated waves.

frequency-generation process $2\omega_y - \omega_y \rightarrow \omega_z$ leads to a nonlinear switching of a y polarized fundamental beam into a z polarized beam at the same frequency [47]. This polarization switching scheme was recently realized in quasi-periodically poled LiNbO$_3$ [48].

Here we have considered simultaneous phase matching of two processes, but any arbitrary number of processes can be phase matched. For example, a one-dimensional three-wave-doubler [45], which phase matches co-linearly three second harmonic generation processes of fundamentals beams with wavelengths 1530, 1550, and 1570 nm was designed, fabricated by electric field poling in KTiOPO$_4$ and experimentally tested.

By using different duty cycles, one can shape the spectral response of NLPCs. For example, in [45], it was shown that by choosing different duty cycles in a quasi-periodic three-wave frequency doubler, one can have the strongest doubling efficiency in either the first, or the second, or the third wavelength. Moreover, it was shown in [45] that such a device of length L is more efficient than three periodic NLPCs (with length of $L/3$ for each period). The ability to shape the spectrum using different motifs can be further extended for cascaded processes [49]. For example, we can consider a third harmonic generation process, consisting of two cascaded processes of second harmonic generation $\omega + \omega = 2\omega$ and sum frequency generation $\omega + 2\omega = 3\omega$. Here the generated wave of the second harmonic process is needed to generate the third harmonic. In this case, it might be useful to adiabatically change the efficiencies of the two processes along the NLPC by changing the duty cycles, so that the third harmonic can be generated with higher efficiency [50].

4.2. Two-dimensional design of quasi-periodic NLPC

2D Quasi-periodic NLPC may be required whenever we need to phase match three or more processes, whose mismatch vectors cannot be spanned as a vectorial sum of two base vectors (i.e., they do not belong to a 2D periodic reciprocal lattice). The same design algorithm that was discussed for the 1D case can be also applied here. Considering an arbitrary set of D nonlinear $\chi^{(2)}$ processes, each of the processes is defined through a phase-mismatch vector $\Delta\mathbf{k}^{(j)}$ $[j = 1, \ldots, D]$. The objective is to create an NLPC that will simultaneously phase match all the nonlinear processes. As in the 1D example that was outlined previously, this is done by solving the problem at a D-dimensional space and projecting the solution into the two-dimensional space. The D two-dimensional mismatch vectors $\Delta k^{(j)}$ $[j = 1, \ldots, D]$ are re-arranged as two D-dimensional vectors. We then add $D - 2$ D-dimensional vectors orthogonal to the first two. We then require orthogonality relations in the D-dimensional space, in order to obtain D real-space vectors that will span the real lattice (in 2D, we use only two components of these vectors). A dual grid is used in order to select only part of the points spanned by the base vectors. A detailed discussion for the design of two-dimensional NLPC is given in [33].

The dual-grid-method when applied to two dimensions generates quasi-crystals whose tiles are parallelograms. To create a nonlinear photonic crystal we need to associate a motif with every tile. We have found that one can get relatively high efficiency by simply using circular motifs (having, say $+\chi^{(2)}$) centered at diagonals bisection point of some parallelograms, while the remaining parts of the parallelogram as well as the parallelograms of different size are left unchanged, with $-\chi^{(2)}$. One can then use numerical optimization to find the optimal radii of these circular motifs. We have recently designed and fabricated two different 2D quasi-periodic NLPC for two applications [51]: a multi-directional single frequency doubler ("SHG Fan") and a multi-directional multi-frequency doubler ("Frequency Fan") which is capable of nearly collinear doubling of continuous wave radiation in the optical communication C-band (1530–1570 nm) through angle tuning. The "SHG Fan" was designed to phase match efficiently collinear SHG of 1550 nm at three propagation directions: $0°$, $\pm 20°$. The "Frequency Fan" was designed to phase match efficiently collinear SHG of the wavelengths 1530, 1540, 1550, 1560, and 1570 nm at propagation directions of $-25°$, $-12.5°$, $0°$, $12.5°$, and $25°$, respectively. Using these RLVs and angle tuning it is possible to double (nearly) collinearly the entire communication C-band (1530–1570 nm). Both NPQCs were fabricated using electric field poling of Stoichiometric LiTaO$_3$ (SLT).

The lattice of both devices can be seen in Fig 5(a) and (d), embedded upon a microscope image of a small part of the NPQC. Also seen are their far field diffraction patterns in Fig 5(b) and (e). These patterns represent the shape of the reciprocal lattices for these two NLPCs. To generate the NPLC pattern, every tile of the lattice is associated with a physical building block. For easy fabrication we chose circular motifs centered at the parallelogram's diagonals bisection points in which the nonlinear tensor component is given at a positive value – positive nonlinear polarization $+\chi^{(2)}$. The background is made with negative polarization $-\chi^{(2)}$. We used a numerical optimization procedure to find the best motifs radii for each tile, to give the best efficiencies for the desired processes. The best results for both devices were given for maximal circle motif within the largest of the parallelograms (6.9 µm radius for the SHG Fan and 4 µm radius for the Frequency Fan) and no circle motifs at all within the other parallelograms. The devices were tested [51] and showed very good agreement to the theoretical predictions.

5. Random, or short-range order nonlinear photonic crystals

For many years it was believed that nonlinear frequency conversion should be done in ordered nonlinear crystals.

In 2004, Baudrier-Raybaut et al. [15] showed that disordered polycrystalline materials can be also used for efficient nonlinear three wave mixing process. They used ZnSe polycrystalline disordered samples, consisting of a large number of single-crystal domains with random orientations, random shapes and random sizes. Conversion efficiency from near infrared to mid-infrared by difference frequency generation was 20 times more efficient than that obtained in an ordered ZnSe single crystal. The process in the ordered crystal was not phase matched, whereas the process in the polycrystalline material was terms as "random phase matching". Whereas ZnSe is suitable for mid-infrared processes, strontium barium niobate (SBN) [52] was proposed earlier as a disordered nonlinear material for visible and near-infrared processes. Non-collinear phase matched second harmonic generation was demonstrated in disordered SBN [14]. This was followed by demonstration of broadband frequency conversion of ultrashort pulses in [53]. The effects of disorder and domain size were studied by Vidal and Martorell [54]. Artificially designed 2D nonlinear crystals, in which random rotations were applied to the unit cell, were used [55] to broaden the spectral and angular acceptance bandwidth in frequency conversion applications, and for cascaded third harmonic generation [56].

We can analyze the effect nonlinear mixing in a random or short-range-order nonlinear photonic crystal, by considering an example of second harmonic generation in a simple one-dimensionally modulated device, having N identical ordered sections of length l. The disorder is attributed to random phase ϕ_m that is accumulated between the ordered sections. This is a simplified version of a 1D polycrystalline crystal, where all the domains were assumed to have identical length l. The second harmonic field can be calculated using Eq. (6):

$$E_{2\omega}(L) = -\frac{\omega d_{ij}}{n_{2\omega}c}E_\omega^2 \frac{e^{i\Delta kl}-1}{\Delta k}\sum_{m=1}^{m=N} e^{i\phi_m} \ . \quad (32)$$

The term that multiplies the summation depends on the phase mismatch in the small section of length l, through the expression $\frac{e^{i\Delta kl}-1}{\Delta k}$. In the phase matched case, $\Delta k = 0$, this expression is simply equal to l, but even in the non phase matched case, if this relatively short section is of the same order as the coherence length, L_c, we can have reasonable contribution to the generated wave. The different contributions are now summed, each one with its corresponding random phase. The second harmonic intensity will be proportional to

$$\left|\sum_{m=1}^{m=N} e^{i\phi_m}\right|^2 = N + \sum_{m=1,k=1,k\neq m}^{m=N,k=N} e^{i(\phi_m-\phi_k)} \ . \quad (33)$$

The summation on the r.h.s. includes $N(N-1)$ terms. If N is very large and we have uniform random distribution of phases ϕ_m, then this term is averaged to zero. This means that the total second harmonic power is N times that of a single section of length l. On the other hand, if

we have non-phase-matched interaction in a long ordered crystal of length Nl, most of the second harmonic light suffers destructive interference, and only a short section whose length is L_c at most will contribute constructively to the output second harmonic. Hence If $l \approx L_c$, the random or short-range order NLPC is N times more efficient than an ordered crystal. Note that the crystal is not really "random", since the build up of the field is made in short ordered sections of length l. Therefore, this device should be regarded as a short range order NLPC.

It is also interesting to consider the case of an ordered crystal with phase-matched interactions. This can be still treated using Eq. (32), for the special case in which all phases ϕ_m are equal. In that case, the term in Eq. (33) is $N + N(N-1) = N^2$, which will result in much higher efficiency with respect to the short-range order NLPC. Another conclusion we can derive from this simple analysis is that the intensity conversion efficiency in short-range order NLPCs scales linearly with the crystal length [15], whereas in the case of a perfectly phase matched NLPC it scales with the square of the crystal length.

6. Advanced nonlinear photonic crystals

6.1. Radial symmetric nonlinear photonic crystals

There are additional "ordered" structures that do not exhibit translation symmetry. One recent example is the annular symmetry frequency converter. This structure consists of a set of concentric rings, alternating between $+d_{ij}$ and $-d_{ij}$. The normalized, space-dependent part of the nonlinear coefficient can be written analytically as a sign function of a radial cosine $g(r) = \text{sign}[\cos(\frac{2\pi r}{\Lambda})]$, where $r = \sqrt{x^2 + y^2}$. This kind of structure is fundamentally different than the lattice-based nonlinear photonic crystals, which have continuous translation symmetry: translating the frequency converters in a direction perpendicular to the input pump wave usually does not change the power of the generated waves. In contrary to that, the radial nonlinear photonic crystal possesses only continuous rotational symmetry and no translation symmetry. The Fourier transform of an infinite annular structure with a period Λ consists of concentric impulse rings with a period of $\frac{2\pi m}{\Lambda}$. If the Ewald sphere intersects with one of these rings the interaction is phase-matched.

We have produced an annular binary structure poled on SLT by electric field poling with a period of 7.5 μm and an active size of 8.75×5 mm, [57], as shown in Fig. 5(h) and (j). Also seen is the far field diffraction pattern in Fig. 5(i). Similar structures were also studied by Wang et al. [58]. The effect of phase mismatch was studied by measuring the temperature dependent second harmonic generation of a Nd:YLF laser through this device. Whereas the first order, collinear phase matching exhibited a sharp, sinc-like dependence on temperature, with full width at half

maximum of 4.5 °C, the non collinear second order phase matched SHG showed negligible temperature dependence in the range of 100–200 °C. The reason is that in the Fourier space, we have continuous lines (rings), rather than discrete points that are obtained for lattice-based NLPCs. Therefore, changing the operating temperature will simply bring the second harmonic propagation vector to a new point on the ring. The low dependence of the annular structure on phase mismatch can be useful for easing the restrictions on exact period length for specific processes when working non co-linearly. A slight change in the period will only result in a slight change of the walk-off angle and not in a sharp efficiency change.

It was shown that by transverse phase matching [59,60], the annular periodic structure supports the generation of second-harmonic conical waves or Bessel beams, which propagate within the nonlinear crystal and eventually evolve into rings at the far field. It was also shown that spatio-temporal toroidal waves can be generated in the annular periodic structure using counter-propagating ultrashort pump pulses.

The periodic annular photonic structure is only one specific example of a diverse family of radial photonic structures displayed in Fig. 15. Fig. 15b shows a radial symmetry nonlinear photonic crystal consisting of concentric rings with radii that are given by a quasi-periodic sequence.
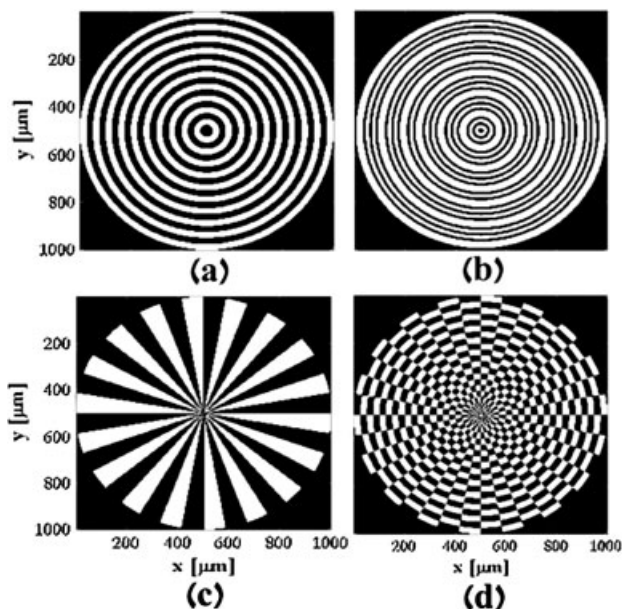

Figure 15 Family of radial photonic structures. The black and white areas denote negative and positive signs of nonlinear coefficients, respectively. (a) Periodic annular photonic structure characterized by period Λ. (b) Aperiodic continuous radial photonic crystal characterized by several periods Λ_n. (c) Discrete periodic radial photonic crystal characterized by azimuthal angle ϕ. (d) Discrete periodic radial photonic crystal characterized by azimuthal angle ϕ and radial period Λ.

This structure can be designed to support arbitrary non-linear processes in any direction [61]. Whereas the structures in Figs. 15a,b have continuous radial symmetry, those in Figs. 15c,d have discrete radial symmetry. Fig. 15c has only azimuthal dependence, whereas Fig. 15d has both azimuthal and radial dependence, and is the analog of two-dimensional Cartesian nonlinear photonic crystal [16,18] in cylindrical coordinates. Nonlinear interactions within these structures were studied in two orientations, transverse and longitudinal, in [61].

6.2. Nonlinear photonic crystals for beam transformation

Quadratic nonlinear photonic crystals are often used for frequency conversion, and in that case usually the pump and generated waves are assumed to be plane waves or Gaussian beams. In this subsection we consider a different aspect that is enabled by these devices, namely the possibility to transform the spatial properties of optical beams. Two dimensional modulation of the nonlinear coefficient enables to control the phase and amplitude of the second harmonic wave along the transverse coordinate [62]. This enables to engineer the wavefront of the second harmonic wave [63]. Here we discuss two specific examples of nonlinear deflection [64] and the generation of optical vortex beams [19].

Nonlinear deflection was recently demonstrated by using a special two-dimensional modulation of the nonlinear coefficient, which consists of a set of symmetric arcs that form a periodic pattern in the propagation direction and a chirped pattern in the transverse direction [64]. The spatial modulation of the nonlinear coefficient to create a symmetric structure is described by $g(r) = \text{sign}[\cos(2\pi f_x x + 2\pi f_{yy} y^2)]$, i.e. a periodic function in the x coordinate and a chirped function in the y coordinate. This structure enables continuous non-collinear phase matching in two symmetric directions (with respect to x) simultaneously. An anti-symmetric deflector that deflects light only in one direction is described by $g(r) = \text{sign}[\cos(2\pi f_x x - 2\pi f_{yy} y^2)]$. Changing the pump wavelength simply changes the angle of the generated second harmonic beam, as shown in Fig. 16. Hence, the deflected second harmonic beam is controlled by the pump wavelength and the phase matching conditions.

The structure was realized in a 0.5 mm thick z-cut MgO-doped stoichiometric lithium tantalate crystal, which was electric-field poled. With poling period of 20.4 μm in the X direction and chirp parameter $f_{yy} = 5 \times 10^{-4}$ μm^{-2} in the Y direction, we have observed continuous angular deflection of the second harmonic wave up to 2.3° by varying the pump wavelength from 1545 nm to 1536 nm at 150 °C. Similar results were obtained by varying the crystal temperature from 125 °C to 180 °C at 1540 nm pump wavelength. The experimental results are reported in detail in [64].

Optical vortices are light waves possessing a phase singularity. The Poynting vector of such beams contains an azimuthal component, causing energy flow around the
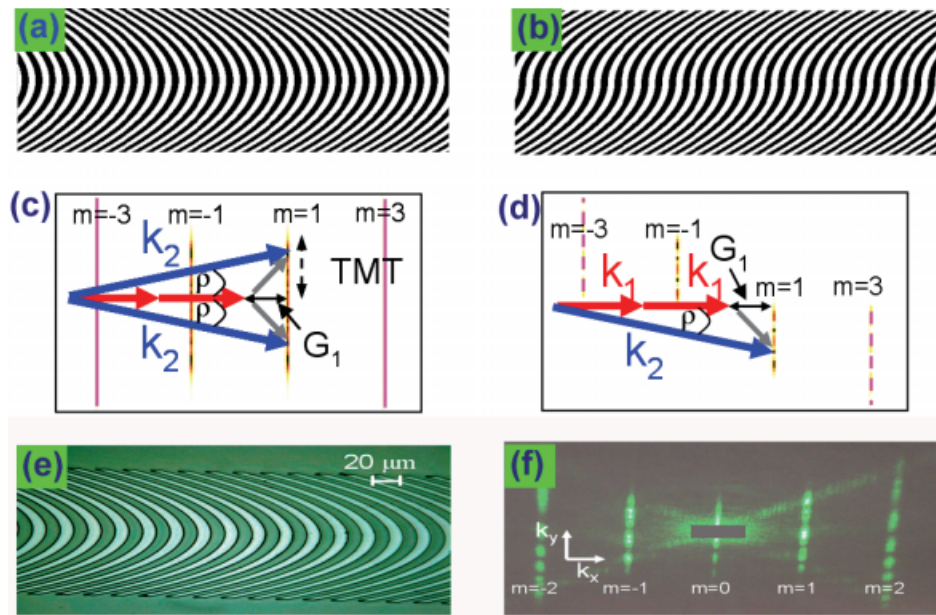
Figure 16 (online color at: www.lpr-journal.org) Nonlinear all-optical deflector [64]. (a) and (b) are the nonlinear patterns for a symmetric and anti-symmetric deflector; (c) and (d) are their corresponding Fourier spectrum, where TMT denotes transverse matching tolerance. (e) is a microscope picture of the mask that was used for producing the symmetric deflector and (f) is the far-field diffraction pattern of the symmetric deflector.

singularity [65] and a ring-shaped intensity profile. Generation of optical vortex beams from a non-vortex fundamental beam by an optical frequency conversion process, taking place within a twisted nonlinear photonic crystal was proposed in [19]. This conversion is done without any first-order linear refractive optics. In order to nonlinearly generate a vortex beam one needs to modulate the nonlinear coefficient also in all three dimensions. The nonlinearity as a function of space should obey

$$g(\mathbf{r}) = \frac{\Delta k}{m(z + \frac{l\theta}{\Delta k})} . \qquad (34)$$

The axial component of this structure function is a periodic modulation in z and is essentially regular m^{th} order quasi-phase-matching. Similarly, the transverse component of the structure function breaks the infinitesimal rotational symmetry, so angular momentum needs to be conserved up to some quasi-angular momentum related to the structure. Therefore, the outcome of a nonlinear wave mixing in such a structured material can result in a radiation which possesses orbital angular momentum which is different than the sum of angular momenta of the pump beams (unlike with a rotationally invariant setup). This allows the generation of a vortex beam from a non-vortex beam.

Realization of this structure requires three dimensional modulation of the nonlinear coefficient at micron-scale resolution. Presently, the available methods to modulate the nonlinear coefficient are planar methods, which allow modulation of only two out of the three needed dimensions. A possible solution for constructing such devices is by electric-field poling of ferroelectric materials into thin nonlinearly modulated planar plates and stacking them together. The stacking could be made in the material polarization direction (the Z direction). This structure should be used when the pump field is linearly polarized in the same direc-

tion as the material polarization, utilizing the largest available nonlinear tensor component. Another option would be to stack thin ferroelectric plates at the beams propagation direction (the X direction). For a topological charge which is equal to the phase matching order $m = l$, all the plates would have the same poling pattern - where half of the plain is positively poled and they would be stacked together with a relative angular shift. Here, however, the material and field polarizations would be perpendicular, utilizing the d_{22} tensor component (which exists in trigonal 3 m crystals, e.g. LiNbO$_3$). Both options would be challenging to implement since each plate should have a thickness of just a few microns.

7. Discussion and summary

In this paper, three wave mixing processes in periodic, quasi-periodic and random nonlinear photonic crystals were analyzed. The main emphasis was on one-dimensional and two-dimensional modulation of the second-order susceptibility, which is currently feasible in various nonlinear materials, e.g. ferroelectrics and semiconductors.

In the case of periodic structures, the efficiency of the nonlinear interaction is governed by the choice of the lattice and the nonlinear motif. Whereas a one-dimensional NLPC has essentially a single type of lattice type (a set of equally-spaced parallel lines) and motif (a strip having nonlinear coefficient with opposite sign than that of the background), the two-dimensional NLPCs offer rich selection of lattice types (the five fundamental 2D Bravais lattices, as well as more sophisticated lattices such as the honeycomb lattice) and motif shapes (circular, hexagonal square, etc.).

Quasi-periodic nonlinear photonic crystals extend the phase matching possibilities beyond the basic limitations

of the modulation dimensions. For example, whereas a one-dimensional periodic NLPC is efficient only for integer multiples of a fundamental phase mismatch value, any set of wave-vectors can be designed to be efficient in a quasi-periodic structure. Similarly, whereas a 2D periodic structure is efficient only for phase mismatch values that are integer combination of two fundamental vectors in a 2D periodic NLPC, a 2D quasi-periodic structure can be designed to be efficient in any arbitrary set of 2D vector combinations. We have outlined a systematic procedure for designing a real-space NLPC, based on phase matching requirements in the reciprocal space [13].

Short range order nonlinear photonic crystals are gaining a lot of interest recently, after it was realized that in some circumstances they can provide higher efficiency than ordered (but not phase-matched) crystals [15]. Moreover, they have wide spectral acceptance bandwidth, which can be useful for converting ultrashort pulses [53]. Whereas the first studies were made on naturally occuring structures such as poly-crystalline ZnSe and SBN, recent results [55] demonstrated the advantages of engineered "random" nonlinear devices. We have analyzed these structures using a simple model and showed that the conversion efficiency in these structures scales with the crystal's length (whereas in ordered and phase matched structures, it scales with the square of the crystal length).

Quadratic nonlinear photonic crystals were traditionally used for frequency conversion, and in that case usually the pump and generated waves were assumed to be plane waves or Gaussian beams. However, the ability to spatially modulate the quadratic nonlinear coefficient with high resolution enables new possibilities. Some of the interesting prospects are in controlling the spatial and polarization properties of optical beams. This enables to transform a zeroth order Gaussian beam to a higher order Hermite-Gaussian beam, Bessel beam [59,66] or a vortex beam [19], as well as to rotate the polarization [46] or change the propagation direction [29,64] of the beam. The various new applications that were discussed here indicate that in addition to their traditional use for frequency conversion, quadratic nonlinear photonic crystals are excellent and flexible tools for all-optical processing of optical beams. It is also interesting to note that the concepts of quasi-periodic and random phase matching are now considered in other regimes of nonlinear optics, such as for selectively enhancing the generation of specific high harmonic waves [67].

Ady Arie received the B. Sc. degree in mathematics and physics from the Hebrew University of Jerusalem, Israel, in 1983 and the M. Sc. degree in physics and Ph. D. degree in engineering from Tel-Aviv University, Tel-Aviv, Israel, in 1986 and 1992, respectively. Between 1991 and 1993, he was a Wolfson and Fulbright Postdoctoral Scholar in the group of Prof. Robert L. Byer at Ginzton Laboratory, Stanford University, Stanford , CA. In 1993 he joined the Department of Physical Electronics, School of Electrical Engineering in the Faculty of Engineering, Tel-Aviv University. Since 2006, he is a Professor of electrical engineering. His research in the last years is in the areas of nonlinear optics and high resolution spectroscopy.

Noa Voloch received the B. Sc. degree from the Israel Institute of Technology (Technion), Haifa, Israel, in 2004 and the M. Sc. degree from Tel- Aviv University, Tel-Aviv, Israel, in 2007, both in physics. She is currently pursuing her Ph. D. degree in electrical engineering at Tel-Aviv University.

References

[1] J. A. Armstrong, N. Bloembergen, J. Ducuing, and P. S. Pershan, Interactions between light waves in a nonlinear dielectric, Phys. Rev. **127**, 1918–1939 (1962).

[2] M. M. Fejer, G. A. Magel, D. H. Jundt, and R. L. Byer, Quasi-phase-matched second harmonic generation – tuning and tolerances, IEEE J. Quantum Electron. **28**, 2631–2654 (1992).

[3] M. Yamada, N. Nada, M. Saitoh, and K. Watanabe, First-order quasi-phase matched LiNbO$_3$ waveguide periodically poled by applying an external field for efficient blue second-harmonic generation, Appl. Phys. Lett. **62**, 435–436 (1993).

[4] S. Moscovich, A. Arie, R. Urneski, A. Agronin, G. Rosenman, and Y. Rosenwaks, Noncollinear second-harmonic generation in sub-micrometer-poled rbtiopo4, Opt. Express **12**(10), 2236–2242 (2004).

[5] C. Canalias and V. Pasiskevicius, Mirrorless optical parametric oscillator, Nature Photon. **1**, 459–462 (2007).

[6] L. A. Eyres, P. J. Tourreau, T. J. Pinguet, C. B. Ebert, J. S. Harris, M. M. Fejer, L. Becouarn, B. Gerard, and E. Lallier, All-epitaxial fabrication of thick, orientation-patterned GaAs films for nonlinear optical frequency conversion, Appl. Phys. Lett. **79**, 904–906 (2001).

[7] M. Houe and P. D. Townsend, An introduction to methods of periodic poling for second-harmonic generation, J. Phys. D, Appl. Phys. **28**, 1747 (1995).

[8] M. Jäger, G. I. Stegeman, W. Brinker, S. Yilmaz, S. Bauer, W. H. G. Horsthuis, and G. R. Möhlmann, Comparison of quasi-phase-matching geometries for second-harmonic generation in poled polymer channel waveguides at 1.5 μm, Appl. Phys. Lett. **68**(9), 1183–1185 (1996).

[9] V. Pruneri and P. G. Kazansky, Frequency doubling of picosecond pulses in periodically poled d-shape silica fibre, Electron. Lett. **33**(4), 318–319 (1997).

[10] R. Kashyap, G. J. Veldhuis, D. C. Rogers, and P. F. Mckee, Phase-matched second-harmonic generation by periodic poling of fused silica, Appl. Phys. Lett. **64**(11), 1332–1334 (1994).

[11] S. N. Zhu, Y. Y. Zhu, and N. B. Ming, Quasi-phase-matched third-harmonic generation in a quasi-periodic optical superlattice, Science **278**, 843 (1997).

[12] K. Fradkin-Kashi, A. Arie, P. Urenski, and G. Rosenman, Multiple nonlinear optical interactions with arbitrary wave vector differences, Phys. Rev. Lett. **88**(2), 023903 (2001).

[13] R. Lifshitz, A. Arie, and A. Bahabad, Photonic quasicrystals for nonlinear optical frequency conversion, Phys. Rev. Lett. **95**(13), 133901 (2005).

[14] A. R. Tunyagi, M. Ulex, and K. Betzler, Noncollinear optical frequency doubling in strontium barium niobate, Phys. Rev. Lett. **90**(24), 243901 (2003).

[15] M. Baudrier-Raybaut, R. Haidar, P. Kupecek, P. Lemasson, and E. Rosencher, Random quasi-phase-matching in bulk polycrystalline isotropic nonlinear materials, Nature **432**, 374–376 (2004).

[16] V. Berger, Nonlinear photonic crystals, Phys. Rev. Lett. **81**(19), 4136–4139 (1998).

[17] N. G. R. Broderick, G. W. Ross, H. L. Offerhaus, D. J. Richardson, and D. C. Hanna, Hexagonally poled lithium niobate: a two-dimensional nonlinear photonic crystal, Phys. Rev. Lett. **84**(19), 4345–4348 (2000).

[18] A. Arie, N. Habshoosh, and A. Bahabad, Quasi phase matching in two-dimensional nonlinear photonic crystals, Opt. Quantum Electron. **39**, 361–375 (2007).

[19] A. Bahabad and A. Arie, Generation of optical vortex beams bynonlinearwave mixing, Opt. Express **15**(26), 17619–17624 (2007).

[20] S. F. Mingaleev and Y. S. Kivshar, Self-trapping and stable localized modes in nonlinear photonic crystals, Phys. Rev. Lett. **86**, 5474 (1996).

[21] D. N. Christodoulides, F. Lederer, and Y. Silberberg, Discretizing light behaviour in linear and nonlinear waveguide lattices, Nature **424**, 817–823 (2003).

[22] S. Somekh and A. Yariv, Phase-matchable nonlinear optical interactions in periodic thin films, Appl. Phys. Lett. **21**(4), 140–141 (1972).

[23] C. L. Tang and P. L. Bey, Phase matching in second harmonic generation using artificial periodic structures, IEEE J. Quantum Electron. **9**(1), 9–17 (1973).

[24] M. Bertolotti, Wave interactions in photonic band structures: an overview, J. Opt. A, Pure Appl. Opt. **8**, S9–S32 (2006).

[25] R. W. Boyd, Nonlinear Optics, 2nd ed. (Academic Press, San Diego, 2003).

[26] A. Chowdhury, C. Staus, B. F. Boland, T. F. Kuech, and L. McCaughan, Experimental demonstration of 1535 1555-nm simultaneous optical wavelength interchange with a nonlinear photonic crystal, Opt. Lett. **26**, 1353 (2001).

[27] N. G. R. Broderick, R. T. Brafalean, T. M. Monro, D. J. Richardson, and C. M. de Sterke, Temperature and wavelength tuning of second-, third-, and fourth-harmonic generation in a two-dimensional hexagonally poled nonlinear crystal, J. Opt. Soc. Am. B **19**, 2263 (2002).

[28] S. Saltiel and Y. S. Kivshar, Phase matching in nonlinear $\chi^{(2)}$ photonic crystals, Opt. Lett. **25**, 1204–1206 (2000).

[29] S. M. Saltiel and Y. S. Kivshar, All-optical deflection and splitting by second-order cascading, Opt. Lett. **27**, 921 (2002).

[30] C. Kittel, Introduction to Solid State Physics, 7th ed. (Wiley, New York, 1995).

[31] S. M. Russell, P. E. Powers, M. J. Missey, and K. L. Schepler, Broadband mid-infrared generation with two-dimensional quasi-phase-matched structures, IEEE J. Quantum Electron. **37**, 877 (2001).

[32] C. Giacovazzo, H. L. Monaco, G. Artioli, D. Viterbo, G. Ferraris, G. Gilli, G. Zanotti, and M. Catti, Fundamentals of Crytallography, 2nd ed. (University Press, Oxford, 2002).

[33] A. Arie, A. Bahabad, and N. Habshoosh, Nonlinear interactions in periodic and quasi-periodic nonlinear photonic crystals, in: Ferroelectric crystals for Photonic Applications, edited by P. Ferraro, S. Grilli, and P. D. Natale (Springer Verlag, Berlin Heidelberg, 2009), Chap. 10.

[34] T. Ellenbogen, A. Arie, and S. M. Saltiel, Noncollinear double quasi phase matching in one-dimensional poled crystals, Opt. Lett. **32**, 262–264 (2007).

[35] M. H. Chou, K. R. Parameswaran, M. M. Fejer, and I. Brener, Multiple-channel wavelength conversion by use of engineered quasi-phase-matching structures in LiNbO$_3$ waveguides, Opt. Lett. **24**, 1157–1159 (1999).

[36] D. Shechtman, I. Blech, D. Gratias, and J. W. Cahn, Metallic phase with long-range orientational order and no translational symmetry, Phys. Rev. Lett. **53**(20), 1951–1953 (1984).

[37] R. Merlin, K. Bajema, R. Clarke, F. Y. Juang, and P. K. Bhattacharya, Quasiperiodic gaas-alas heterostructures, Phys. Rev. Lett. **55**(17), 1768–1770 (1985).

[38] K. Fradkin-Kashi and A. Arie, Multiple-wavelength quasi-phase-matched nonlinear interactions, IEEE J. Quantum Electron. **35**, 1649–1656 (1999).

[39] J. Liao, J. L. He, H. Liu, J. Du, F. Xu, H. T. Wang, S. N. Zhu, Y. Y. Zhu, and N. B. Ming, Red, yellow, green and blue – four-color light from a single, aperiodically poled LiTaO$_3$ crystal, Appl. Phys. B, Lasers Opt. **78**, 265–267 (2004).

[40] R. T. Bratfalean, A. C. Peacock, N. G. R. Broderick, K. Gallo, and R. Lewen, Harmonic generation in a two-dimensional nonlinear quasi-crystal, Opt. Lett. **30**, 424–426 (2005).

[41] B. Ma, T. Wang, Y. Sheng, P. Ni, Y. Wang, B. Cheng, and D. Zhang, Quasiphase matched harmonic generation in a two-dimensional octagonal photonic superlattice, Appl. Phys. Lett. **87**(25), 251103 (2005).

[42] N. de Bruijn, Algebraic theory of penrose's non-periodic tilings of the plane, Proc. K. Ned. Akad. Wet. A **84**, 39–66 (1981).

[43] D. A. Rabson, T. L. Ho, and N. D. Mermin, Aperiodic tilings with non-symmorphic space groups $p2^j gm$, Acta Crystallographica Section A **44**(5), 678–688 (1988).

[44] D. A. Rabson, T. L. Ho, and N. D. Mermin, Space groups of quasicrystallographic tilings, Acta Cryst. A **45**(8), 538–547 (1989).

[45] A. Bahabad, N. Voloch, A. Arie, and R. Lifshitz, Experimental confirmation of the general solution to the multiple phase matching problem, J. Opt. Soc. Am. B **24**, 1916–1921 (2007).

[46] S. Saltiel and Y. Deyanova, Polarization switching as a result of cascading of two simultaneously phase-matched quadratic processes, Opt. Lett. **24**(18), 1296–1298 (1999).

[47] A. Bahabad, R. Lifshitz, N. Voloch, and A. Arie, Nonlinear photonic quasicrystals for novel optical devices., Philos. Mag. **88**(13–15), 2285–2293 (2008).

[48] A. Ganany-Padowicz, I. Juwiler, O. Gayer, A. Bahabad, and A. Arie, All-optical polarization switch in a quadratic nonlinear photonic quasicrystal, Appl. Phys. Lett. **94**(9), 091108 (2009).

[49] S. M. Saltiel, A. A. Sukhorukov, and Y. S. Kivshar, Multistep parametric processes in nonlinear optics, Progr. Opt. **47**, 1–73 (2005).

[50] S. Longhi, Third-harmonic generation in quasi-phase-matched $\chi(2)$ media with missing second harmonic, Opt. Lett. **32**(13), 1791–1793 (2007).

[51] A. Bahabad, A. Ganany-Padowicz, and A. Arie, Engineering two-dimensional nonlinear photonic quasi-crystals, Opt. Lett. **33**(12), 1386–1388 (2008).

[52] S. Kawai, T. Ogawa, H. S. Lee, R. C. DeMattei, and R. S. Feigelson, Second-harmonic generation from needle-like ferroelectric domains in $Sr_{0.6}Ba_{0.4}Nd_2O_6$ single crystals, Appl. Phys. Lett. **73**(6), 768–770 (1998).

[53] R. Fischer, S. M. Saltiel, D. N. Neshev, W. Krolikowski, and Y. S. Kivshar, Broadband femtosecond frequency doubling in random media, Appl. Phys. Lett. **89**(19), 191105 (2006).

[54] X. Vidal and J. Martorell, Generation of light in media with a random distribution of nonlinear domains, Phys. Rev. Lett. **97**(1), 013902 (2006).

[55] Y. Sheng, J. Dou, B. Ma, B. Cheng, and D. Zhang, Broadband efficient second harmonic generation in media with a short-range order, Appl. Phys. Lett. **91**(1), 011101 (2007).

[56] Y. Sheng, S. M. Saltiel, and K. Koynov, Cascaded third-harmonic generation in a single short-range-ordered nonlinear photonic crystal, Opt. Lett. **34**(5), 656–658 (2009).

[57] D. Kasimov, A. Arie, E. Winebrand, G. Rosenman, A. Bruner, P. Shaier, and D. Eger, Annular symmetry nonlinear frequency converters, Opt. Exp. **14**, 9371–9376 (2006).

[58] T. Wang, B. Ma, Y. Sheng, P. Ni, B. Cheng, and D. Zhang, Large angle acceptance of quasi-phase-matched second harmonic generation in a homocentrically poled LiNBO$_3$, Opt. Commun. **252**(4–6), 397–401 (2005).

[59] S. M. Saltiel, D. N. Neshev, R. Fischer, W. Krolikowski, A. Arie, and Y. S. Kivshar, Generation of second-harmonic conical waves via nonlinear bragg diffraction, Phys. Rev. Lett. **100**(10), 103902 (2008).

[60] S. M. Saltiel, D. N. Neshev, R. Fischer, W. Krolikowski, A. Arie, and Y. S. Kivshar, Spatiotemporal toroidal waves from the transverse second-harmonic generation, Opt. Lett. **33**(5), 527–529 (2008).

[61] N. Voloch, T. Ellenbogen, and A. Arie, Radially symmetric nonlinear photonic crystals, J. Opt. Soc. Am. B **26**(1), 42–49 (2009).

[62] J. Kurz, A. Schober, D. Hum, A. Saltzman, and M. M. Fejer, Nonlinear physical optics with transversely patterned quasi-phase-matching gratings, IEEE J. Sel. Top. Quantum Electron. **8**, 660–664 (2002).

[63] Y. qiang Qin, C. Zhang, Y. yuan Zhu, X. peng Hu, and G. Zhao, Wave-front engineering by huygens-fresnel principle for nonlinear optical interactions in domain engineered structures, Phys. Rev. Lett. **100**(6), 063902 (2008).

[64] T. Ellenbogen, A. Ganany-Padowicz, and A. Arie, Nonlinear photonic structures for all-optical deflection, Opt. Express **16**(5), 3077–3082 (2008).

[65] L. Allen, M. W. Beijersbergen, R. J. C. Spreeuw, and J. P. Woerdman, Orbital angular momentum of light and the transformation of laguerre-gaussian laser modes, Phys. Rev. A **45**(11), 8185–8189 (1992).

[66] S. Saltiel, W. Krolikowski, D. Neshev, and Y. S. Kivshar, Generation of bessel beams by parametric frequency doubling in annular nonlinear periodic structures, Opt. Express **15**(7), 4132–4138 (2007).

[67] A. Bahabad, O. Cohen, M. M. Murnane, and H. C. Kapteyn, Quasi-periodic and random quasi-phase matching of high harmonic generation, Opt. Lett. **33**(17), 1936–1938 (2008).